THE JOURNAL OF PHYSICAL CHEMISTRY C

C: Physical Processes in Nanomaterials and Nanostructures

Composites of Poly(3,4-ethylenedioxythiophene) and CoFe2O4 Nanoparticles: Composition Influence on Structural, Electrical and Magnetic Properties

Matías Lanús Mendez Elizalde, Carlos Acha, Fernando Victor Molina, and Paula Soledad Antonel

J. Phys. Chem. C, **Just Accepted Manuscript** • DOI: 10.1021/acs.jpcc.9b11241 • Publication Date (Web): 05 Mar 2020

Composites of Poly(3,4-ethylenedioxythiophene) and $CoFe_2O_4$ Nanoparticles: Composition Influence on Structural, Electrical and Magnetic Properties

Matías Lanús Mendez Elizalde, [†] *Carlos Acha,* [‡] *Fernando V. Molina,* [†] *P. Soledad Antonel* *,[†]

[†] Instituto de Química Física de Materiales, Ambiente y Energía (INQUIMAE) and Departamento de Química Inorgánica, Analítica y Química Física, Facultad de Ciencias Exactas y Naturales, Universidad de Buenos Aires, Ciudad Universitaria, Pabellon II, piso 1, C1428EGA, Buenos Aires, Argentina.

[‡] Laboratorio de Bajas Temperaturas, Departamento de Física, Facultad de Ciencias Exactas y Naturales, Universidad de Buenos Aires and IFIBA (UBA-CONICET), Ciudad Universitaria, Pabellón I, C1428EHA, Buenos Aires, Argentina.

ABSTRACT

Composites of magnetic $CoFe_2O_4$ nanoparticles (MNP) in a Poly(3,4-ethylenedioxythiophene) matrix at different ratios have been synthetized. Composites were characterized by electron microscopy, X-ray diffraction, thermal analysis, electrical conductivity, magnetization and magnetoresistance studies. In the composites the MNP appear clustered, with an interparticle distance essentially constant, but where two regimes are distinguished for cluster separation: for high MNP concentrations an intercluster separation similar to the interparticle distance is found, while for low MNP contents the distance between clusters is larger than the interparticle separation. The electrical conductivity increases with polymer content, but being always far lower than general effective medium theory expectations. This indicates that the effect of MNP effect on polymer conduction is probably related to the generation of mechanical stress by both introducing additional scattering centers and by producing different arrangement of the polymer chains, compared with the pure PEDOT. The magnetization studies reveal the existence of the RKKY interaction, which couples ferromagnetically the MNP located in a cluster, while the dipolar interaction dominates the interaction between clusters. Magnetoresistance was studied for these composites, with a maximum value close to 0.7% at 0.8 T for the lowest polymer content. The magnetoresistance correlates very well with the reversible part of the magnetization, indicating that its possible origin should be associated with polymer mechanical deformation due to the magnetic-field-induced rotation of the MNP.

INTRODUCTION

Composite materials based on conducting polymers and magnetic nanoparticles (MNP) have received much attention in the last years.[1–11] Conducting polymers, in one hand, have interesting chemical, conducting, mechanical and optical properties leading to a high number of proposed applications.[12–15] In particular, Poly(3,4-ethylenedioxythiophene (PEDOT) is highly interesting because of its excellent environmental stability,[16] high electrical conductivity[17] and transparency in the doped state.[18] On the other hand, MNP are also highly interesting materials, due to their potential applications in different fields.[19,20] In particular, spinel ferrite nanoparticles have been intensively investigated and, among them, cobalt ferrite ($CoFe_2O_4$) is especially interesting because it is a hard material from the magnetic point of view and has moderate saturation magnetization, exhibiting also excellent stability.[21,22] Also, it has promising application for microelectronic devices, actuators and transducers. Thus, by combining conducting polymers and MNP it is possible to obtain materials with high magnetic susceptibilities and high electrical conductivities, giving rise to applications in non-linear optics, electromagnetic interference shielding, microwave absorption, electrochemical supercapacitors, ion adsorption and electrocatalysis, between others.[8,11,23–28] All these applications underline the importance of the study of these composites from an applied point of view, besides the fundamental interest. In particular, there are few reports concerning composites based on PEDOT and MNP, which studies include microwave absorption behavior,[28] adsorption of heavy metal ions[29] and catalytic performance.[25] Other interesting property that show conducting polymers, including PEDOT, is the magnetoresistance effect (OMAR) [30–34], mainly associated with the spin correlations between different carriers, while the standard magnetoresistance (MR) refers to the phenomenon in which the electrical resistance of a material changes when an external magnetic field is applied to it.

This latter effect was also studied in MNP, in particular magnetite[35] and ferrites.[36,37] It is proposed that materials that show MR could be applied in spintronics, electronics, computer memory, storage technology and magnetoresistance sensors.[34,38–40] For these reasons, there are several challenges in the design of novel and suitable magnetic materials that show improved magnetoresistance effect. Within these materials, composites based on conducting polymers and MNP are attractive candidates for this end,[41,42] although to the present their magnetoresistance effect has not been study deeply. Is the MR effect related to the local magnetic field generated by the MNP? Do the metallic nature of the polymeric matrix affect the magnetic interactions and then influences the MR effect? How can be maximized the MR? To answer these questions it is necessary to perform an exhaustive and complete physicochemical characterization, in order to have tools allowing to synthetize a material with the desired properties; this is to say, to tune the physicochemical properties through the synthetic route employed.[43,44] To the best of our knowledge, there are relatively few reports that show the dependence of the final properties of PEDOT-based composites (such as electrical conductivity, magnetic properties and morphology) on the conducting polymer:MNP molar ratio in the composites.[3,41,45] In a recent study[46], the thickness of the polymer shell of core-shell magnetite-PEDOT microspheres was tuned by varying the magnetite:monomer molar ratio. Moreover, in order to have a better understanding of the influence of the composition on the final properties, it is important to study the magnetic interactions between the different components in the composites. To the present, and to the best of our knowledge, there are no reports concerning the type and magnitude of the magnetic interactions in composites based on PEDOT conducting polymer and $CoFe_2O_4$ nanoparticles. The change in the type and magnitude of the magnetic interactions with the composite

composition is a fundamental study to gain insight, also, in the potential application of these materials in the magnetoresistance field.

In this work, composites based on PEDOT and MNP of $CoFe_2O_4$ were chemically synthetized, by varying the EDOT:MNP molar ratio in the feed solution in order to obtained materials with different compositions. Morphology, crystallinity, electrical conductivity, magnetoresistance and magnetic properties, focusing in the type and magnitude of the interactions, were thoroughly studied and analyzed, in order to understand their correlations with the overall electric and magnetic properties.

MATERIALS AND METHODS

AR grade chemicals, supplied by Sigma-Aldrich, and high purity water (18 MΩ cm) from a Milli-Q system were employed throughout. Ethylenedioxythiophene (EDOT) was used as received.

Synthesis of cobalt ferrite nanoparticles

The synthesis of $CoFe_2O_4$ nanoparticles was performed following Antonel et al.[47] Briefly, 22.25 mL of a solution containing 0.450 M $FeCl_3.6H_2O$ and 0.225 M $CoCl_2.6H_2O$ (2:1 Fe(III)-Co(II) molar ratio), in 0.4 M HCl, was added dropwise to 200 mL of 1.5 M NaOH under constant and high speed mechanical stirring. The synthesis temperature was set at 80º C, using a water-jacketed reaction vessel with a circulating thermostatic bath. Dark brown $CoFe_2O_4$ nanoparticles precipitated immediately after the first drops of the Fe(III)-Co(II) solution. The temperature of synthesis and the high-speed mechanical stirring were kept constant during the addition of the cationic solution. After the addition of this solution, the reaction media was maintained at 80º C, at high-speed stirring, for 2 hrs. The $CoFe_2O_4$ nanoparticles were separated

by centrifugation at 12000 G during 20 minutes at room temperature. The pellet was washed with Milli-Q water, repeating the cycles of washing-centrifugation until neutral pH of the supernatant was reached (about 10 times). Finally, the $CoFe_2O_4$ nanoparticles were dried using a vacuum oven at 40º C during 24 hrs.

Synthesis of $CoFe_2O_4$-PEDOT composites and PEDOT

$CoFe_2O_4$-PEDOT composites were synthesized following Ohlan et al.,[48] with some modifications. First, $CoFe_2O_4$ nanoparticles were added to a 0.1 M dodecylbenzenesulfonic acid (DBSA) solution (used as both protecting agent and acid media), in a $CoFe_2O_4$:DBSA molar ratio of 0.33. In order to efficiently disperse the MNP and to allow DBSA adsorption onto them, strong mechanical stirring and ultrasound treatment were applied for 30 minutes. This was carried out by placing the recipient containing the DBSA solution and MNP in an ultrasonic bath (Testlab, model TB04), operating with a power of 160 watts and a frequency of 40 kHz. After that, a brown emulsion was obtained. Then, ethylenedioxithiophene (EDOT) monomer (in molar ratios with respect to $CoFe_2O_4$, r_{EDOT}, of 2, 5 and 10) was added keeping the reaction mixture in the same conditions for 1 h. Finally, ammonium persulfate (APS), in a molar ratio of 1:1 with respect to EDOT, was added, and the reaction mixture was kept 3 h always under ultrasound treatment and mechanical stirring. The product was demulsified with an equal volume of isopropyl alcohol. The blue precipitate obtained was separated by centrifugation at 15000 G during 10 minutes at 17º C, washed with ethanol and MilliQ water to remove the excess of reactants and oligomers, and dried at room temperature for 24 h.

As it was mentioned above, the synthesis was performed for different values of the molar ratio in the feed:

$$r_{EDOT} = \frac{n_{EDOT}}{n_{CF}} \qquad (1)$$

where n_{EDOT} and n_{CF} are the mole numbers of EDOT monomer and $CoFe_2O_4$, respectively.

For comparison, the PEDOT-DBSA polymer was synthesized in the same conditions of $CoFe_2O_4$-PEDOT composites described above but MNP were not incorporated in the reaction media.

X-Ray diffraction (XRD) measurements

X-Ray powder diffraction analysis of nanoparticles and composites was performed with a Philips X-Pert diffractometer using Cu Kα radiation (λ = 0.154056 nm); the average crystallite size was determined with the Scherrer equation:

$$d_C = \frac{A\,\lambda}{\beta \cos(\theta)} \qquad (2)$$

where A is a shape factor, taken here as 0.9, β is the full width at half maximum of the peak and θ is the corresponding Bragg angle.

Electron microscopy studies

The particle size and morphology of particles and composites were studied by Scanning Electron Microscopy (SEM) and Transmission Electron Microscopy (TEM). SEM analysis was performed using a Zeiss Supra 40 Gemini microscope equipped with and EDS detector. The samples were prepared by placing a small amount of each solid (nanoparticles or composites) in one side of a carbon tape. EDS measurements were carried out in the same experiment. TEM observation was performed using a Transmission Electron Microscope Philips EM 301. High Resolution Transmission Electron Microscopy (HR-TEM) brightfield imaging was performed using a Transmission Electron Microscope Philips CM200 UT with LaB6 thermoelectric emission filament and ultra-Twin lens with a resolution of 0.19 nm. Each material (nanoparticles or composites) was suspended in acetone and approximately 10 μL of each suspension were dripped on a TEM grid and dried prior to insertion to TEM column.

Thermal analysis

Thermogravimetric analysis (TGA) of $CoFe_2O_4$ nanoparticles, CoFe2O4-PEDOT composites and PEDOT polymer was performed using a thermobalance TG-DTA 50 simultaneous Shimadzu. The TGA thermograms were recorded for 10-20 mg of each sample at a heating rate of 10º C/min in the temperature range of 25-800º C under air atmosphere.

Fourier transform infrared spectroscopy (FTIR) characterization

The infrared (IR) measurements of composites, nanoparticles and polymer were performed using a FTIR Nicolet 8700 spectrometer, in the range 400-4000 cm^{-1}, with a resolution of 4 cm^{-1}. The samples were pressed into pellets prepared dispersing 0.5 mg of each one in 150 mg of KBr. For each sample, 32 scans were accumulated.

Electrical conductivity measurements

The DC conductivity of the different samples was measured on pressed circular pellets (1 cm diameter) using a Teq-03 (Nanoteq, Buenos Aires, Argentina) potentiostat under computer control. Following Ohm's law, a known current was applied and the potential difference was measured and averaged during 120 s. The pellet thickness was measured with a caliper to compute the conductivity.

Magnetization and magnetoresistance studies

A Lakeshore 7400 Vibrating Sample Magnetometer (VSM) was used for recording magnetization curves at room temperature. The samples were prepared by packing with Teflon tape 10-20 mg of each composite. Also, two different primary remanent magnetization curves were measured at room temperature: isothermal remanent magnetization (IRM) and DC demagnetization (DCD) curves. For the IRM experiments, initially the sample was totally demagnetized at room temperature. Then, a small external field *H* was applied and subsequently

removed, and the remanence was measured, M_{IRM}. The process was repeated increasing the external magnetic field up to 1 T. At this field, the remanence reaches its saturation value, $M_{IRM}(\infty)$. For the DCD curves, first the sample was saturated. Then, a small external field H, in the direction opposite to the magnetization, was applied. Finally, the external field was switched off and the remanence was measured, M_{DCD}. This procedure was repeated, increasing the field H, until the saturation in the opposite direction is reached.

The resistance of the different samples was also measured in the presence of an applied magnetic field. Contacts using copper wires (100 μm of diameter), attached with silver paste to the pellets and disposed in a planar configuration, were used to perform standard 2 and 4 terminals techniques, with similar results in both cases. In this way, the contact resistance and the thermoelectric voltages of each terminal can be ruled out, disregarding their contribution to the measurement of the bulk resistance. In order to avoid overheating, measurements were performed with a Keithley 2614B Source Meter by applying 10 ms square voltage pulses at 1 Hz rate and by measuring the current during the 50% last part of the pulse. Details of this technique can be found elsewhere[49]. Magnetic field was varied between - 0.7 T and 0.7 T and incremented at a rate of 5.0 mT s^{-1}. To minimize slow drifts possibly caused by polymer degradation, as suggested by Lupton et al.,[50] the external magnetic field was applied after the electric signal was stabilized. Also, multiple magnetoresistance measurements were carried out and averaged.

Percent magnetoresistance (MR%) was calculated following

$$MR\% = \frac{R_H - R_0}{R_0} \times 100 \qquad (3)$$

where R_H is the resistance at the applied magnetic field, H, and R_0 is the resistance in the absence of a magnetic field.

RESULTS AND DISCUSSION

Particle size and composites morphology.

The morphology of the cobalt ferrite particles obtained here corresponds to a spheric-like shape aggregated in clusters, very similar to those of Antonel et al.[3] and Muñoz Resta et al.,[45] as they were prepared with the very same technique. In Figs. 1a to d TEM images of $CoFe_2O_4$-PEDOT composites are shown. TEM image of pure $CoFe_2O_4$ nanoparticles, after the same treatment employed for the polymerization of EDOT, is observed in Fig. 1a. The particle size, as verified by TEM imaging with the aid of the ImageJ software, was found to be $d_P = (14 \pm 3)$ nm, very similar to the size of $CoFe_2O_4$ nanoparticles without treatment. This result indicates that DBSA effectively protects $CoFe_2O_4$ nanoparticles from the reaction medium. Besides, the particle size is within the range of monodomain magnetic particles, which for cobalt ferrite falls between a minimum of 7-9 nm[22,51] and a maximum of about 60-70 nm.[52,53]

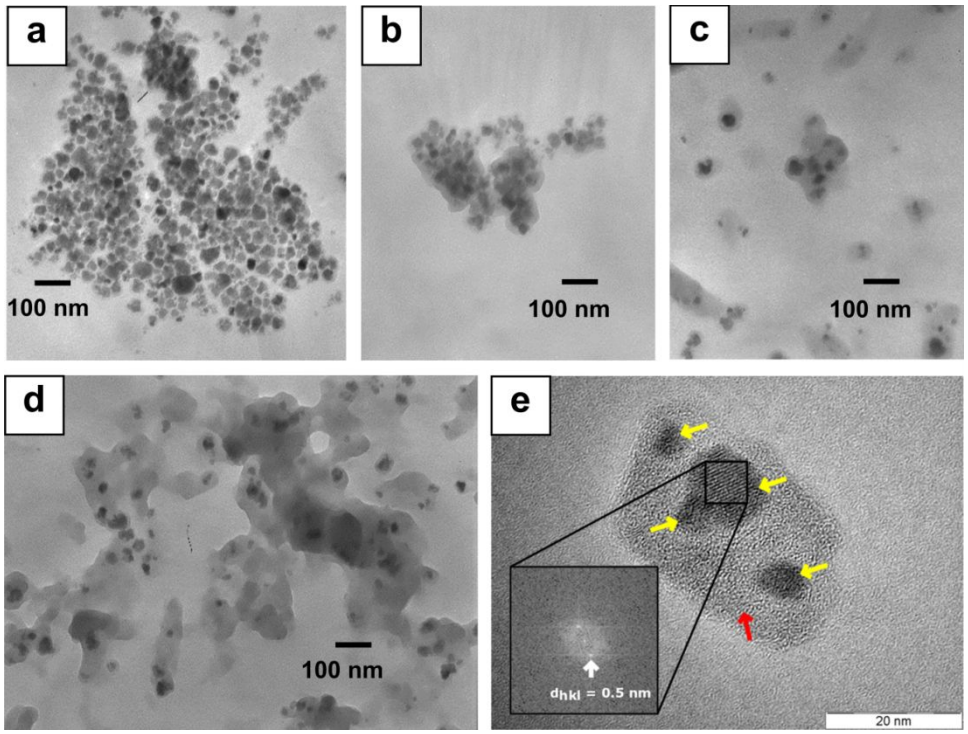

Fig. 1. TEM and HR-TEM images of $CoFe_2O4$ nanoparticles and $CoFe_2O_4$-PEDOT composites: (a) TEM image of $CoFe_2O_4$ nanoparticles after polymerization treatment (without monomer); (b) TEM image of composite with r_{EDOT} = 2 (c) TEM image of composite with r_{EDOT} = 5; (d) TEM image of composite with r_{EDOT} = 10; (e) HR-TEM image of composite with r_{EDOT} = 5, yellow arrows: MNP; red arrow: PEDOT. Inset: FFT analysis of a 40 nm^2 area of a $CoFe_2O_4$ nanoparticle region.

Also, in Fig 1 it is clear that high r_{EDOT} favors the dispersion of the nanoparticles as they appear more separated with the increase in r_{EDOT}. It is worth mentioning that these MNP act as catalyst for EDOT polymerization, since the polymerization yield increases significantly when they are present in the reaction medium. From (b) to (d) there is a marked change in the composite morphology. For r_{EDOT} = 2 (Fig. 1b) the polymer appears mostly covering the MNP, whereas for r_{EDOT} = 10 the MNP appear dispersed in a large polymer matrix, the material with r_{EDOT} = 5 showing an intermediate morphology. This is interpreted considering that, first, PEDOT is produced preferably around $CoFe_2O_4$ nanoparticles, and for higher r_{EDOT} the conducting polymer grows further giving rise to a homogeneous polymeric matrix with the nanoparticles aggregated in clusters, these in turn dispersed in an approximately uniform way. These features were also observed previously for $CoFe_2O_4$-PANI[3] and $CoFe_2O_4$-PPy[45] composites.

Fig. 1e shows a typical HR-TEM image of a composite with r_{EDOT} = 5. The nanoparticles (dark gray, indicated by yellow arrows) are surrounded by the polymer matrix (gray region, indicated by the red arrow). The high resolution of this image evidence the crystallinity of the nanoparticles in contrast with the amorphous nature of the polymer.

Fast Fourier Transform (FFT) analysis of the nanoparticle (Fig. 1e inset) shows a d_{hkl} of 0.5 nm corresponding to the (1 1 1) spinel family of lattice planes.

The morphology of some of the obtained materials, as observed by SEM, is shown in Fig. 2a to e; Fig. 2e shows an image of PEDOT without particles for comparison.

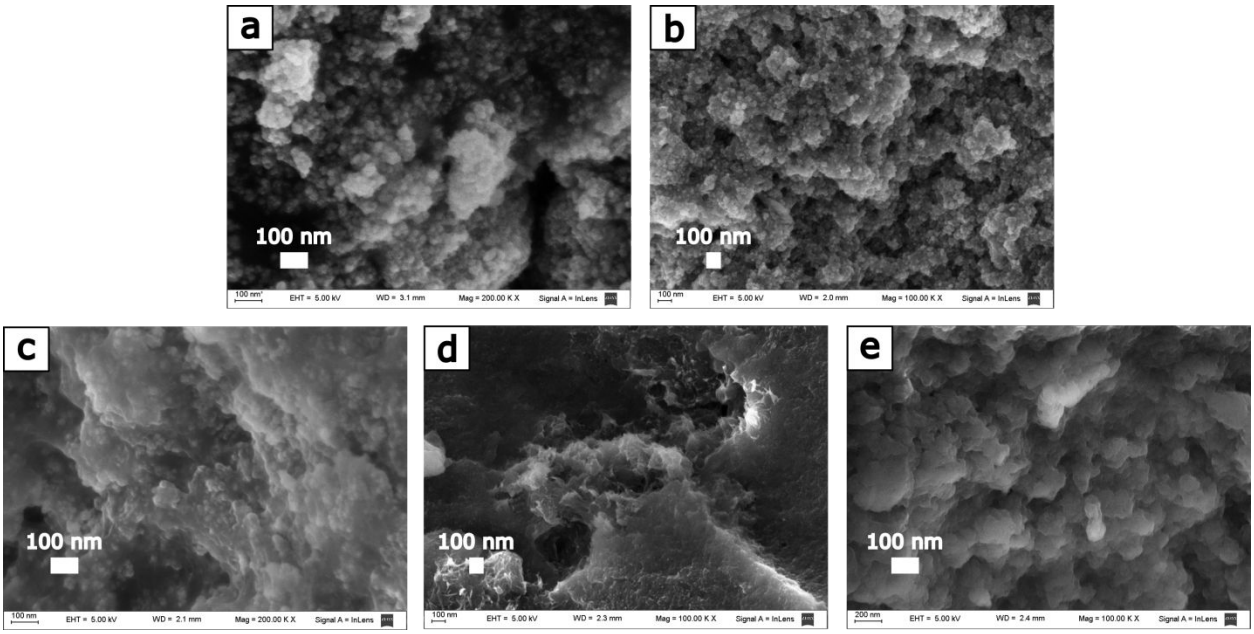

Fig. 2. SEM images of $CoFe_2O_4$-PEDOT composites: (a) $CoFe_2O_4$ nanoparticles after polymerization treatment (without monomer); (b) r_{EDOT} = 2; (c) r_{EDOT} = 5; (d) r_{EDOT} = 10; (e) PEDOT.

Similarly to TEM observation, different morphologies are found for low and high values of r_{EDOT}. The composite with very low polymer content (r_{EDOT} = 2, Fig. 2b) shows a morphology that is very similar to that of bare $CoFe_2O_4$ nanoparticles (Fig. 2a). When increasing the PEDOT content (r_{EDOT} = 5, Fig. 2c), composites have a relatively smooth topography, as a consequence of being dominated by the polymer presence. Finally, for high polymer content (r_{EDOT} = 10) the materials show a more regular surface, very similar to the pure polymer (Fig. 2e).

The chemical composition of the MNP was verified from SEM-EDS measurements (not shown), resulting in a Fe:Co molar ratio of 2:1, thus confirming that the product obtained was effectively $CoFe_2O_4$.

As it was shown in Fig. 1, the MNP appear aggregated in clusters in the composites with PEDOT. In order to have an estimation of the particle-particle separation inside each cluster, the distances between MNP were measured with the aid of the ImageJ software and the resulting histograms are presented in Fig. 3a-c, with the corresponding log-normal distributions. For each composite, approximately 100 particle-particle separations inside each cluster were measured. In the case of the composite with r_{EDOT} = 10, TEM images show that the distance between clusters is significantly larger than the particle-particle separation inside each cluster while is not the case for $r_{EDOT} \leq 5$. So, in this case, about 75 distances between clusters were measured and the resulting histograms are shown in Fig. 3d, also with the corresponding log-normal distribution.

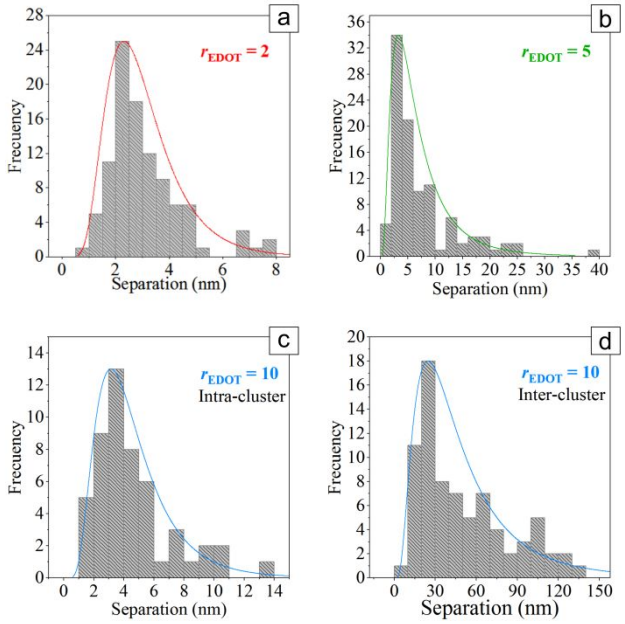

Fig. 3. Particle-particle separation for $CoFe_2O_4$-PEDOT composites with: (a) r_{EDOT} = 2; (b) r_{EDOT} = 5; (c) r_{EDOT} = 10 (intra-cluster) and (d) r_{EDOT} = 10 (inter-cluster).

From the log-normal distributions for the particle-particle separation inside clusters in the composites with different r_{EDOT}, first the mean values and the standard deviations were calculated. The obtained values are: 3 nm (standard deviation = 2 nm) for the composite with r_{EDOT} = 2, 7 nm (standard deviation = 4 nm) for the composite with r_{EDOT} = 5 and 5 nm (standard deviation = 3 nm) for the composite with r_{EDOT} = 10. Also the modes were calculated, obtaining a value of 3 nm for the composite with r_{EDOT} = 2, 6 nm for the composite with r_{EDOT} = 5 and 4 nm for the composite with r_{EDOT} = 10. These results suggest that, within experimental error, the distance between MNP inside clusters remain approximately constant and is independent of r_{EDOT}. On the other hand, the cluster-cluster separation increases noticeably in the composite with r_{EDOT} = 10, having a mean value of 50 nm (standard deviation = 30 nm) and a mode value of 40 nm. These results indicate that in the composites the MNP are aggregated in clusters, with an interparticle separation distance essentially constant (~3-6 nm) but where two regimes can be distinguished for the intercluster separation: for high MNP concentration (r_{EDOT} = 2) a particle dominated composite, with an intercluster separation similar to the interparticle distance, while for a low MNP content (r_{EDOT} = 10), a polymer-dominated material is obtained, where the distance between clusters is clearly larger than the interparticle distance. That means that, for low r_{EDOT} ($r_{EDOT} \leq 5$) the polymer appears mostly covering the MNP giving as a result an interparticle separation approximately constant. In other words, the distances between MNP are all very similar in composites with $r_{EDOT} \leq 5$ and are determined by the PEDOT layer that grows covering the MNP. On the other hand, for r_{EDOT} = 10 there is a higher monomer concentration in the synthesis medium, resulting in faster growth of PEDOT. Initially, the polymer appears covering the ferrite particles resulting in clusters as before and, after that, the excess monomer present polymerizes around the clusters, resulting in larger separation between them.

Crystalline structure

The XRD patterns of the nanoparticles obtained are shown in Fig. 4, where a typical inverse spinel pattern is observed (ICDD 03-0864, JCPDS 22-1086) with the space group *Fd3m*, very similar to that of Fe_3O_4.[22,54] The ferrite lattice parameter was determined using the (311) peak and was found to be a = b = c = 8.369 Å, which is close to the values reported for $CoFe_2O_4$ nanoparticles.[55–57] Besides, the obtained value of 8.369 Å is smaller than 8.395 Å which corresponds to the lattice parameter of bulk $CoFe_2O_4$.[22] This indicates that in $CoFe_2O_4$ nanoparticles there are more defect sites in comparison with bulk $CoFe_2O_4$, fact that could be explained taking into account the high area / volume ratio in nanostructured systems. The diameter of the crystallites, d_c, prepared here was estimated through Equation (2) using the (311) peak, resulting in d_c = 15.4 nm which is in agreement with the TEM measurements and with the previous reported results.[22,47]

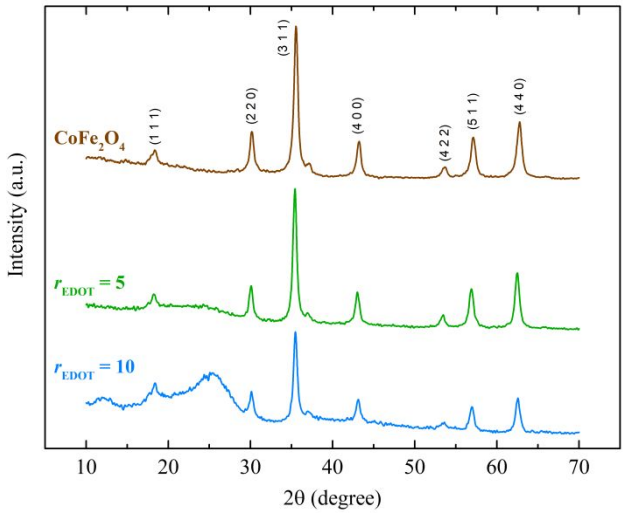

Fig. 4. XRD diagram/patterns of $CoFe_2O_4$ nanoparticles and composites for different r_{EDOT} ratios. Nanoparticles synthesized at 80 ºC reveals an inverse spinel structure.

Fig. 4 also shows the XRD patterns for composites with r_{EDOT} = 5 and r_{EDOT} = 10. For smaller r_{EDOT}, the diffractograms do not shown the presence of the amorphous phase associated with the polymer, and are essentially identical to the one shown for pure $CoFe_2O_4$ nanoparticles. It is clearly observed that for a polymer dominated material (r_{EDOT} = 10), a broad diffraction band around 2θ = 25 degree, characteristic of the low crystallinity of the polymer, is observed. Also, these results are consistent with TEM and SEM observations, which show particle-dominated composites for r_{EDOT} = 2 and polymer-dominated materials for r_{EDOT} = 10. Note that for r_{EDOT} = 5 the polymer band is present but very weak, consistent with a transition between NMP and polymer dominated materials. Comparing this results with those obtained for composites of $CoFe_2O_4$ nanoparticles and PANI[3] or PPy[45], with PANI or PPy a higher amount of polymer is incorporated in the materials, giving as a result polymer-dominated composites even with small values for the respective monomer:ferrite molar ratios, r_{ANI} or r_{Py} (5 in the case of PANI[3] and 3.5 in the case of PPy[45]). This result is consistent with the lower polymerization rate for EDOT compared with pyrrole and aniline.

Thermal decomposition and composite composition

To study the thermal decomposition of the resulting composites and to gain insight into their composition, thermogravimetric analysis (TGA) in air was conducted (Fig. 5); it is observed that PEDOT-DBSA is completely decomposed by oxidation and the ferrite particles undergo only a small mass loss, whereas the composites give intermediate results, thus confirming the composite formation. The features in Fig. 5 can be explained as follows: first, when increasing the temperature T, an initial mass loss is observed, attributable to removal of water from the material; this loss ends at about 250 ºC, where the curves are almost leveled. At higher temperatures, a pronounced decrease is observed, corresponding to polymer decomposition,

starting between ~ 307 ± 5 ºC (as estimated from the curve derivative, not shown), with a second step at about 500 ºC, and ending at ~ 600 ºC for PEDOT-DBSA. This is in agreement with literature reports, where PEDOT decomposition occurs mainly in the range ~ 300 - 450 ºC,[58] but mass loss is observed up to ~ 600 ºC.

On the other hand, for $CoFe_2O_4$-PEDOT composites the polymer decomposition starts at 260 ± 10 ºC (independent of composition within experimental error), and takes place up to ~ 450-480 ºC, without a discernible second stage. The differences comparing with the PEDOT-DBSA case can be attributed to a catalytic effect of the ferrite particles on the polymer decomposition.

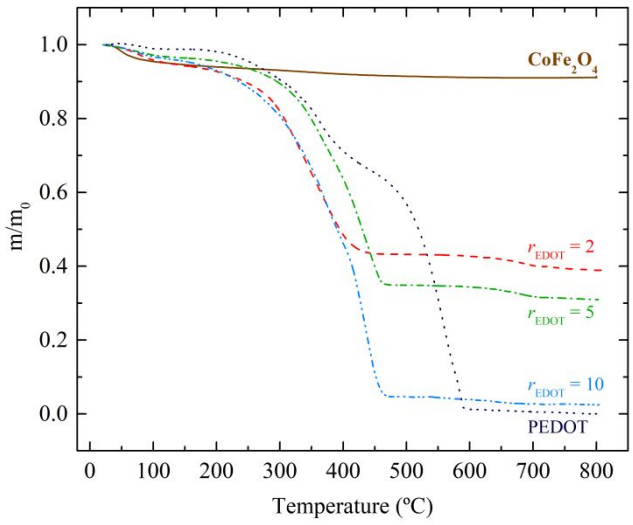

Fig. 5. TGA measurements of cobalt ferrite, PEDOT and composites, plotted as relative mass (m/m_0) as a function of temperature.

Pure ferrite particles show, after some water elimination, a small decrease probably due to loss of surface hydroxyl groups. From the TGA results, the composites composition can be estimated, assuming that the mass loss at T < 250 ºC is due to water elimination, that the remaining mass at T = 800 ºC corresponds to the ferrite particles with no polymer remaining, and introducing a correction for the mass change of the cobalt ferrite particles between 25 and 800 ºC. The results

for the $CoFe_2O_4$ mass fraction in the composite, f_{CF}, and the measured polymer/ferrite molar ratio, r_m are presented in Table 1.

Table 1. Composites composition as found by thermogravimetric analysis

Feed composition, r_{EDOT}	Measured composition, r_m	Cobalt ferrite mass fraction, f_{CF}
2.0	2.1 ± 0.1	0.45 ± 0.02
5.0	3.2 ± 0.3	0.34 ± 0.03
10.0	57 ± 9	0.13 ± 0.02

Electrical conductivity

The electrical conductivity of the composites depends of the monomer-ferrite ratio, being in the range 10^{-5}-10^{-3} S cm^{-1} with a monotonous decrease as the ferrite contents increases, as it can be observed in Table 2. On the other hand, PEDOT prepared in the same conditions as the nanocomposites, gives a conductivity of 0.3 S cm^{-1}. This value is similar to several results reported for PEDOT obtained using APS or Fe(III) as oxidizing agents. For example, Choi et al.[58] found bulk conductivities for PEDOT also synthesized with APS as oxidant and DBSA of 1-10 S cm^{-1}; Morvant et al.[59] prepared thick films of PEDOT, obtaining in-situ conductivities in the range 0.2-13.0 S cm^{-1}, depending on growth conditions; Corradi et al.[60] synthesized PEDOT at different reaction temperatures, using Fe(III) as oxidizing agent, and in this case the maximum electrical conductivity achieved was of ~ 5 S cm^{-1}.

The electrical conductivity values for the composites show that the presence of the MNP highly affects the polymer electrical conductivity, since even those with the highest r_{EDOT} gives composites with low conductivities. Nevertheless, the minimum electrical conductivity value achieved (approximately 10^{-5} S cm^{-1}) suggests that, down to the lower r_{EDOT} explored, PEDOT retains an electrical conductivity path, indicating that the polymer is able to percolate through the material.

Table 2. Room pressure and temperature conductivities of PEDOT and composites with different r_{EDOT} ratios.

Sample		Conductivity / S cm^{-1}
Composite feed composition, r_{EDOT}	2.0	$(2.2 \pm 0.8) \times 10^{-5}$
	5.0	$(4.5 \pm 1.5) \times 10^{-4}$
	10.0	$(6.0 \pm 3.0) \times 10^{-3}$
PEDOT (w/o MNP)		0.3 ± 0.1

Additionally, it should be mentioned that the conductivity of the composites is far away from the values expected from the general effective media (GEM) theory, which quantitatively describes the conductivity of a binary mixture as a function of the conductivities and the volume fraction of each component.[61,62] The observed behavior indicates the strong effect that the MNP have on the conductivity of PEDOT as even a small fraction (r_{EDOT} = 10) decreases the conductivity of the composite far below from the expected values determined by the GEM model (≈1/50). The same effect, with similar values, was observed for PANI and Fe_3O_4 or $CoFe_2O_4$

composites.[1,3] This indicates that the inclusion of MNP has a long range effect which is probably related to the generation of mechanical stress and to a change in the electrical mobility of carriers, by both introducing additional scattering centers and by producing different arrangement of the polymer chains, compared with the pure PEDOT. This last fact is due to the initial growth of the polymer around the MNP, as suggested by SEM images, resulting in less crystallinity and thus a lower electrical conductivity.

IR Spectroscopy

Fig. 6 shows the IR spectra of PEDOT, $CoFe_2O_4$ nanoparticles and composites PEDOT-$CoFe_2O_4$ with different r_{EDOT} ratio.

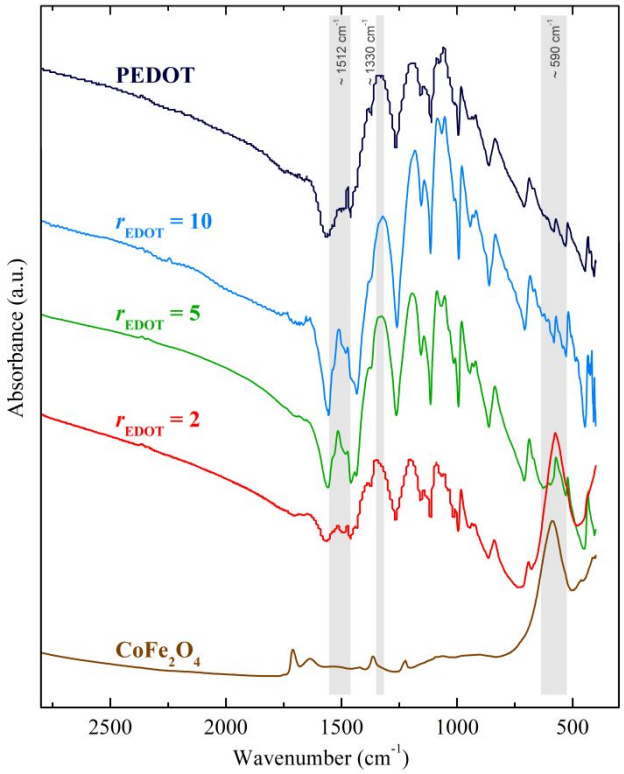

Fig. 6. IR spectra of PEDOT, $CoFe_2O_4$ nanoparticles and composites PEDOT-$CoFe_2O_4$ with different r_{EDOT} ratio.

The IR response of PEDOT (Fig. 6, top) has been reported by several authors.[48,58,63,64] The most relevant bands of the spectra shown in Fig. 6 will be discussed in the following. The vibrational band at around 1512 cm^{-1} corresponds to C=C or C-C ring stretching of the thiophene ring and the one around 1330 cm^{-1} corresponds to C=C or C-C ring stretching of the quinoid structure of the thiophene ring. Vibrational bands at 1190 cm^{-1}, 1142 cm^{-1} and 1055 cm^{-1} are due to C-O-C bond stretching in the ethylenedioxy group. The band around 920 cm^{-1} is originated from the ethylenedioxy ring deformation. Vibration modes of the C-S bond in the thiophene ring are also seen at 980 cm^{-1}, 835 cm^{-1} and 685 cm^{-1}. In the spectrum of cobalt ferrite (bottom), on the other hand, besides surface OH vibrations ca. 3500 cm^{-1} (not shown) and other minor bands, the main lattice band at 590 cm^{-1} is clearly visible. In the composite spectra, this band shows decreasing intensity as r_{EDOT} increases, as expected. The absence of additional peaks in the range between 1600 cm^{-1} and 1800 cm^{-1}, which would indicate carbonyl groups formation by oxidation, demonstrates that the overoxidation of the polymer can be excluded. There are some differences between the polymer bands in pure PEDOT spectrum and those in the composites, which indicates that some interaction of ferrite nanoparticles with polymer chains takes place. The most prominent change is observed in the vibrational band at 1512 cm^{-1}, which corresponds to C=C or C-C ring stretching of the thiophene ring: first, a displacement to 1520 cm^{-1} is observed for the composite with $r_{EDOT} = 2$; also, this band undergo a splitting, giving a second one at 1470 cm^{-1}, with the A_{1470} / A_{1510} ratio (absorbance ratio) increasing with ferrite content.

Magnetization behavior and magnetic interactions

Fig. 7 shows the mass magnetization, M, as a function of the magnetic field H for the bare particles and composites, all measured at room temperature.

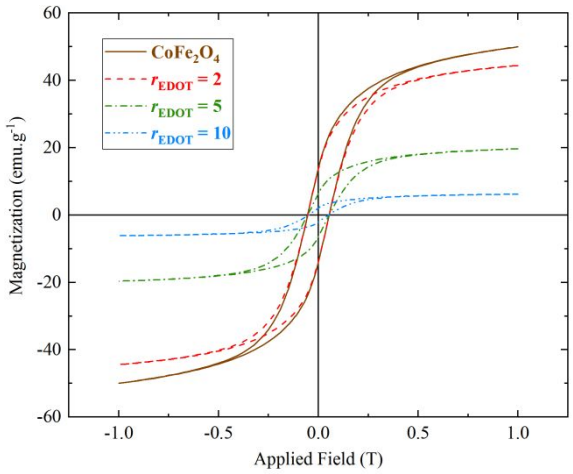

Fig. 7. Magnetization curves of $CoFe_2O_4$ particles and composites with different r_{EDOT} measured at room temperature.

The curve for the bare particles is similar to others reported in the literature,[22,45,47,51] showing hysteresis, which reveals ferromagnetic behavior. $CoFe_2O_4$ MNP synthetized and used in this work can be considered as magnetic monodomain particles, since their average size was found to be d_P = (14 ± 3) nm, as it was observed in TEM images. This average size lies between the critical single domain size (70 nm)[52,53] and the superparamagnetic threshold (7-9 nm)[22,51] in the case of $CoFe_2O_4$ MNP. That means that $CoFe_2O_4$ MNP having an average size between 7-9 and 70 nm are expected to be in the monodomain regime, showing a ferromagnetic behavior at room temperature, as it was observed in the magnetization hysteresis loops shown in Fig. 7. The fact that $CoFe_2O_4$ MNP show ferromagnetism at room temperature is due to their high magnetocrystalline anisotropy[22,65,66]. Following Muñoz Resta et al.[45], for small and single domain ferromagnetic particles, the coercivity is limited by the net anisotropy of these particles, which includes the magnetocrystalline anisotropy. Moreover, the coercivity is proportional to the anisotropy constant[66], giving as a result that $CoFe_2O_4$ MNP show ferromagnetic behavior at room temperature, result also found by other authors. [3,22,45,47,55,65,67]

The magnetization is referred to the total composite mass, thus the curves have smaller M values as the contents of magnetic particles decreases. In particular, the maximum magnetization reached at H = 1 T, M_{max} (which has not yet reached its saturation value M_s), decreases as the polymer content increases, because PEDOT is essentially a non-magnetic material. M_s can be estimated by fitting the M vs H curve with a simplify law of approach to the saturation:[68]

$$M = M_s\left(1-\frac{a}{H}-\frac{b}{H^2}\right) \qquad (4)$$

where a and b are appropriate constants.

The obtained M_s value for the bare $CoFe_2O_4$ MNP (59 emu g^{-1}) is in accordance to the values published for MNP of similar diameters.[22,45,69] The results for all the composites are listed in Table 3.

Table 3. Coercive field and remanence ratio of cobalt ferrite and composites.

Material	$CoFe_2O_4$	r_{EDOT} = 2	r_{EDOT} = 5	r_{EDOT} = 10
$H_c/10^{-4}$ T	543 ± 6	543 ± 4	541 ± 7	504 ± 7
M_r/M_{max}	0.278 ± 0.003	0.308 ± 0.002	0.326 ± 0.003	0.339 ± 0.003
M_r/M_s	0.233 ± 0.001	0.273 ± 0.002	0.289 ± 0.002	0.304 ± 0.001

Interestingly, although the mass fraction of the MNP for the r_{EDOT} = 2 composite is close to 45% of the composite mass, its M_{max} value is almost 85% of the M_{max} value for the bare particles. Also, for the r_{EDOT} = 5 and r_{EDOT} = 10 composites their M_{max} is higher than the one expected for their mass fraction of MNP. The same conclusions are found if we consider the estimated M_s

values. This result is clearly indicating that the magnetization of the composites is not obeying to a simple mass dilution of the MNP content. Instead, an additional ferromagnetic (FM) interaction should be playing an important role. As the MNP are embedded in PEDOT, which is an electrical conducting material, it is possible to have a Ruderman-Kittel-Kasuya-Yosida (RKKY) mechanism which produces an indirect exchange coupling between the magnetic moment of the MNP through the electrical carriers (holes) of PEDOT. [70]

The RKKY coupling will be intensely ferromagnetic for MNP that are closer than a distance d_{FM} while for longer distances (d), it will oscillate periodically from antiferromagnetic to ferromagnetic and decay as d^3. d_{FM} can be roughly estimated as:

$$d_{FM} = \frac{4.49}{2k_F} = \frac{4.49}{2\left(3\pi^2 n\right)^{1/3}} \qquad (5)$$

where k_F is the Fermi wave vector and n the density of free carriers.

An estimation of the n value for our composites can be done as follows:

As the electrical conductivity is $\sigma = n\mu q$ (where n is the density of carriers, μ their mobility and q the elementary charge), and by considering the span of μ values reported for PEDOT materials[71–73] synthetized with close counter-ions, but discarding those extremely high values, corresponding to samples prepared in a particular way in order to reach the most higher values of electrical conductivities ($\sigma > 6000$ S cm^{-1}), we obtain that:

0.1 cm^2 V^{-1} s^{-1} $\leq \mu \leq$ 10 cm^2 V^{-1} s^{-1},

which, for our measured σ in the case of PEDOT:DBSA (0.3 S cm^{-1}), limits the n values to 2 10^{23} m^{-3} $\leq n \leq$ 2 10^{25} m^{-3}. In this way, we obtain from Equation (5) that 3 nm $\leq d_{FM} \leq$ 13 nm. Within this interval of possible d_{FM} values, this result is in accordance with the observed behavior of M_{max} and M_s for the $r_{EDOT} = 2$ and $r_{EDOT} = 5$ composites. That is, by considering the

distance distribution of MNP for each composite (see Fig. 3), it can be observed that, even for the extreme case of $d_{FM} \approx 3$ nm, a large portion of them will be coupled FM, yielding to a cluster-like magnetic behavior and, concomitantly, to an increase of their M_{max} (or equivalently of M_s). The RKKY influence on the M_s of a magnetic material surrounded by an electrical conducting matrix has been already observed, for example, in $CoFe_2O_4$ MNP interconnected by an Au matrix, where M_s presents an oscillatory damped behavior as a function of the Au width between MNP. [74]

In order to compare more closely the above curves, they are presented in Fig. 8 in the form of relative magnetization, M/M_{max} as a function of the magnetic field. The inset shows the curves in the full range, where it is observed that all the curves merge for high field values.

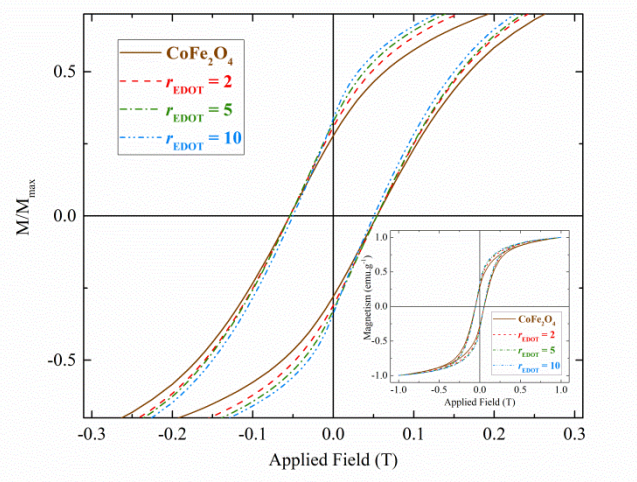

Fig. 8. Normalized magnetization curves for $CoFe_2O_4$-PEDOT composites, for different r_{EDOT}. The insets show the full curves, and the main graphs present an enlargement about $H = 0$.

The main graph shows an enlarged view of the low field region, revealing that the remanence ratio, M_r/M_{max}, increases as the polymer contents increases, and also a relatively small decrease (in terms of the H range) in the coercivity H_c is found for the composite with $r_{EDOT} = 10$. These results suggest that, in terms of coercivity, the magnetic properties of the composites also show

an abrupt change when passing from particle dominated composites (r_{EDOT} = 2) to a polymer-dominated material (r_{EDOT} = 10), as it was observed in SEM and TEM observation and in XRD studies. These results, summarized in Table 3, also support the framework of a RKKY interaction between MNP and mediated by the electrons of PEDOT, already discussed for the M_{max} behavior, indicating that there is a change in the magnetic properties when the particles are included in the composite. Otherwise, if a simple "dilution" effect was taking place all the normalized curves should be coincident. So, the remanence ratio increases with r_{EDOT}, sustaining the presence of FM interactions between the magnetic NP at the expense of the polymer matrix.

To gain insight into the type and strength of interaction between MNP, isothermal remanence magnetization (IRM) and DC demagnetization (DCD) curves, both at room temperature, were measured. The results, well known as Henkel plots,[75] are shown in Fig. 9. The dash line corresponds to Equation (6) and represents the expected behavior for a non-interacting system, as predicted by the Stoner-Wohlfarth model:[76]

$$\frac{M_{DCD}}{M_R(\infty)} = 1 - \frac{2M_{IRM}}{M_R(\infty)} \qquad (6)$$

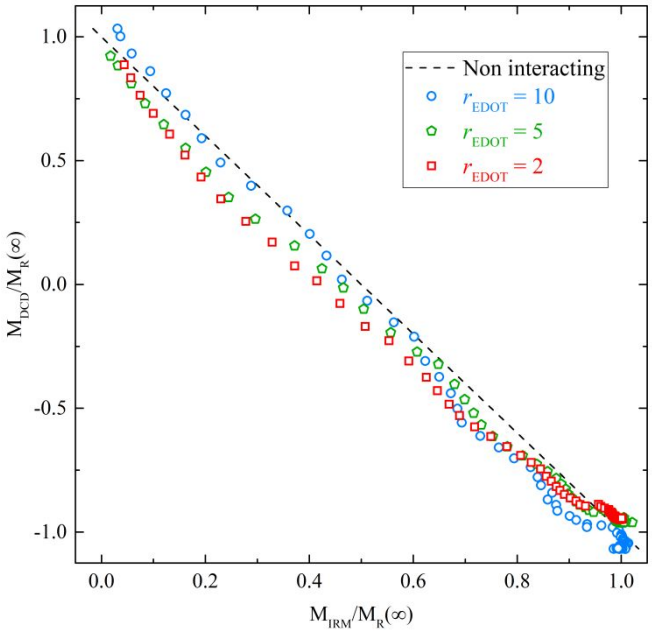

Fig. 9. Henkel Plot for $CoFe_2O_4$-PEDOT composites with different r_{EDOT} ratios.

As can be observed, all the composites show a negative deviation from the dash line that increases with decreasing r_{EDOT} (or the polymer content), indicating that the main interparticle magnetic interaction is dipolar.[77]

This is an interesting result due to the fact that regardless of the existence of a FM coupling between MNP mediated by the RKKY interaction, the dipolar interaction is the dominant one in the magnetization and demagnetization processes.

A possible interpretation of this result can be done considering that the RKKY interaction strongly couples ferromagnetically all the MNP that are at distances less than the estimated interval for d_{FM} (3-13 nm), causing them to act as a single magnetic cluster. In this framework, the IRM and DCD curves would reveal the existence of magnetic dipolar interactions between clusters. In fact, it can be observed that dipolar interactions are weak for the composite with r_{EDOT} = 10, strong for the composite with r_{EDOT} = 2 and have an intermediate magnitude for the

composite with r_{EDOT} = 5. This result is in accordance with the expected spatial dependence of the dipolar interaction on the average distance between magnetic interacting particles, which could then be associated with the mentioned clusters of MNP (see Fig. 3).

From the IRM measurements additional information about the reversible contribution to the magnetization, M_{rev}, can be obtained, by considering the following relation:

$$M_{rev}(H) = M'(H) - M_{IRM}(H) \quad (7)$$

where M' is the magnetization of the first magnetization curve and M_{IRM}, as the remanent contribution, corresponds to the irreversible part of the magnetization. Results for the normalized M_{rev} are shown in Fig. 10. It can be seen that M_{rev} increases with the applied magnetic field for all the composites, being this increment more pronounced up to ~ 0.4 T. Also the increment in M_{rev} with H depends on r_{EDOT}, showing a higher value as the mass fraction of the MNP increases.

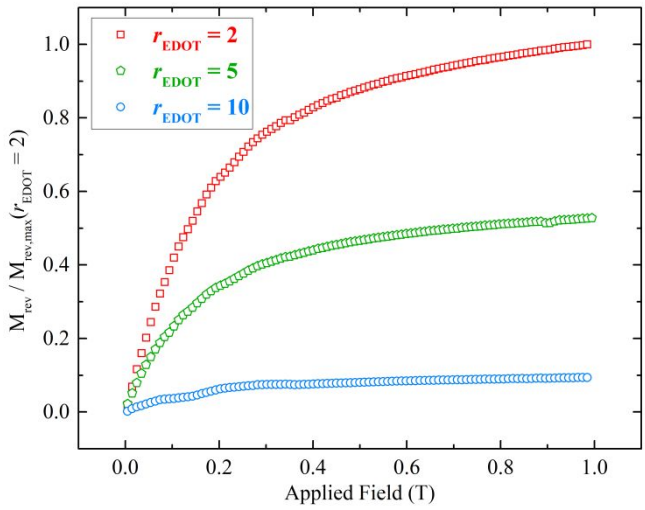

Fig. 10. Normalized reversible magnetization for $CoFe_2O_4$-PEDOT composites with different r_{EDOT} ratios.

Magnetoresistance

Fig. 11 shows *MR*%, computed from Equation (3), of $CoFe_2O_4$-PEDOT composites at room temperature.

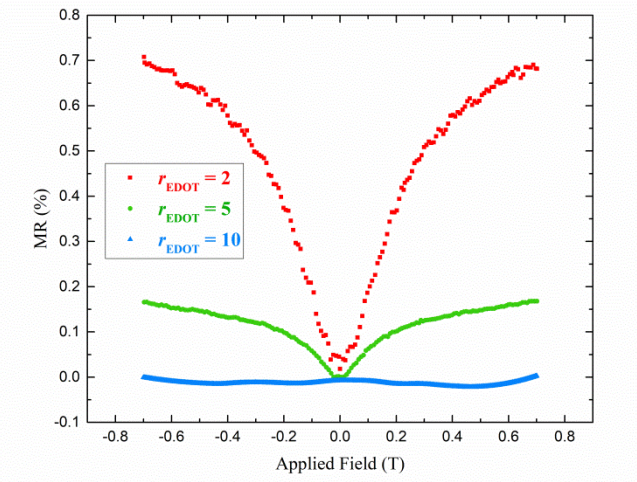

Fig. 11. Magnetoresistance for $CoFe_2O_4$-PEDOT composites with different r_{EDOT} ratios.

MR% depends on r_{EDOT}, being positive, reversible and increasing in value with the applied magnetic field, as already seen by Gu et al. for composites of PANI-magnetite,[42] by Muñoz Resta et al. for composites of PPy-$CoFe_2O_4$,[45] and Klemm et al.[50] for PEDOT:PSS polymer. Furthermore, the magnetoresistance decreases with increasing r_{EDOT} and becomes negligible for pure PEDOT, indicating its correlation with the presence of MNP. *MR*% reached values up to 0.7% for composites with $r_{EDOT} = 2$ while for composites with $r_{EDOT} \geq 2$ the maximum *MR*% is about 0.15 %. Moreover, for the composite with $r_{EDOT} = 2$ there is a linear relationship between de *MR*% and *H*, in the low field region (up to ~ 0.3 T), which favors considering this material as a promising candidate to be applied as a magnetic sensor. To the best of our knowledge this is the first time that magnetoresistance measurements of PEDOT-$CoFe_2O_4$ composites are investigated.

The reversible behavior of *MR*% with the magnetic field and its dependence with the MNP content leads us to consider that its microscopic origin may be related to what generates the

reversible part of the magnetization. Indeed, it should be noted that the shape of *MR*% vs *H* and M_{rev} vs *H* (Fig. 11 and Fig. 10, respectively) is quite similar (at least for the composites with r_{EDOT} = 2 and r_{EDOT} = 5), effectively suggesting that the origin of the observed phenomena is the same in both cases. To better visualize the correlation between the magnetoresistance and the reversible magnetization, the relative magnetoresistance, $MR/MR_{,max}$, vs. the relative reversible magnetization, $M_{rev}/M_{rev,max}$, is presented in Fig. 12.

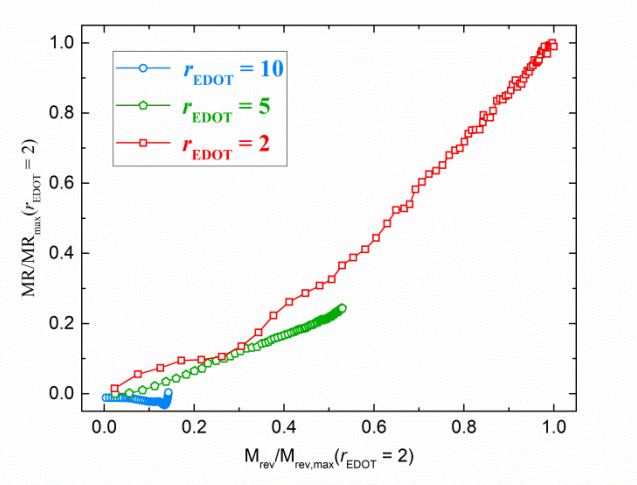

Fig. 12. Normalized Relative Magnetoresistance vs. Relative Reversible magnetization for $CoFe_2O_4$-PEDOT composites with different r_{EDOT} molar ratios.

Fig. 12 shows that for MNP dominated materials (r_{EDOT} = 2) a strong dependence of the normalized MR with normalized M_{rev} is found, whereas for the polymer dominated case (r_{EDOT} = 10) there is practically no effect; r_{EDOT} = 5, as before, shows an intermediate behavior. In this way, Fig. 12 reveals that the M_{rev} dependence of MR% can be scaled for the composites above a minimum concentration of MNP, and confirms that the magnitude of the observed magnetoresistance is a function of the reversible term of the magnetization.

These results give an interesting clue about the microscopic origin of *MR* for these composites. Indeed, the non-hysteretic behavior of *MR* ruled out that the magnetoresistance could be related

to an interaction between the electrical carriers and the magnetic moments of MNP or their local magnetic field. Discarding its direct magnetic origin, but considering its dependence with M_{rev}, the magnetic-field-induced rotation of the MNP can be considered as its possible source. In this context, rotation of NPMs could stretch the polymer chains as well as narrowing their local section, being consistently two contributions that produce a positive magnetoresistance. Further studies are needed to confirm this hypothesis.

Conclusions

Composites based on MNP of $CoFe_2O_4$ and the conducting polymer PEDOT in different molar ratios were synthetized chemically, using DBSA as acid media and nanoparticles protecting agent. In these materials the nanoparticles are aggregated in clusters, and the morphology depends on r_{EDOT}. It was also found that the electrical conductivity of the composites decreases as r_{EDOT} increases, being in the range 10^{-5} – 10^{-3} S cm^{-1}. These values indicates that the inclusion of MNP has a long range effect in the electrical conductivity of PEDOT, which is probably related to the generation of mechanical stress and to a change in the electrical mobility of carriers. From the magnetization experiments it can be concluded that in PEDOT-$CoFe_2O_4$ composites exist a RKKY interaction that strongly couples ferromagnetically all the MNP that are at distances less than the estimated interval for d_{FM} (3-13 nm), causing them to act as a single magnetic cluster, giving as a result an increase in the magnetization of saturation and in the remanence ratio with r_{EDOT}. On the other hand, between magnetic clusters exist dipolar interactions, which magnitude decreases with the increase in r_{EDOT}. The composites also exhibit positive and reversible magnetoresistance, which magnitude increases with the applied magnetic field and decreases with increasing r_{EDOT}, being negligible for pure PEDOT. The applied magnetic field induces the rotation of the MNP, phenomenon that could stretch the polymer

chains as well narrowing their local section, giving as a result an increase in the magnetoresistance with the applied magnetic field. Moreover, for the composite with $r_{EDOT} = 2$ the maximum MR% is 0.7 % and there is also a linear relationship between the MR% and H in the low field region. This last result favors considering this material as a promising candidate to be applied as a magnetic sensor. All the results obtained and the analysis performed in this work allows to have a physical understanding of the magnetic interactions and their relationship with r_{EDOT}, facts that are very important for the future application of these composite materials.

AUTHOR INFORMATION

Corresponding Author

P. Soledad Antonel. Instituto de Química Física de Materiales, Ambiente y Energía (INQUIMAE) and Departamento de Química Inorgánica, Analítica y Química Física, Facultad de Ciencias Exactas y Naturales, Universidad de Buenos Aires. Ciudad Universitaria, Pabellón II, piso 1, C1428EHA Buenos Aires, Argentina. sole@qi.fcen.uba.ar

Author Contributions

The manuscript was written through contributions of all authors. M. L. M. E. performed the experimental part; C. A. devised and supervised IRM, DCD, magnetoresistance and conductivity measurements; M. L. M. E., C. A. and P. S. A. analyzed the results; F. V. M. contributed with the discussions; P. S. A. devised and supervised all the experiments and wrote the manuscript. All authors have given approval to the final version of the manuscript.

ACKNOWLEDGMENT

The authors gratefully acknowledge funding from the Universidad de Buenos Aires (grants 20020130100035BA, 20020170100284BA and 20020120300007BA) and the Agencia Nacional de Promoción Científica y Tecnológica (grants PICT 2014 Nº 2289 and Nº 1194), all of Argentina. The collaborations of A. G. Leyva in the thermogravimetric measurements and of G. Lavorato in HR-TEM measurements are gratefully acknowledged. P. S. A., C. A. and F. V. M are members of the Carrera del Investigador Científico of CONICET.

REFERENCES

(1) Deng, J.; He, C.; Peng, Y.; Wang, J.; Long, X.; Li, P.; Chan, A. S. C. Magnetic and Conductive Fe3O4–Polyaniline Nanoparticles with Core–Shell Structure. *Synth. Met.* **2003**, *139* (2), 295–301. https://doi.org/10.1016/S0379-6779(03)00166-8.

(2) Reddy, K. R.; Park, W.; Sin, B. C.; Noh, J.; Lee, Y. Synthesis of Electrically Conductive and Superparamagnetic Monodispersed Iron Oxide-Conjugated Polymer Composite Nanoparticles by in Situ Chemical Oxidative Polymerization. *J. Colloid Interface Sci.* **2009**, *335* (1), 34–39. https://doi.org/10.1016/j.jcis.2009.02.068.

(3) Antonel, P. S.; Berhó, F. M.; Jorge, G.; Molina, F. V. Magnetic Composites of CoFe2O4 Nanoparticles in a Poly(Aniline) Matrix: Enhancement of Remanence Ratio and Coercivity. *Synth. Met.* **2015**, *199*, 292–302. https://doi.org/10.1016/J.SYNTHMET.2014.12.003.

(4) Yang, C.; Du, J.; Peng, Q.; Qiao, R.; Chen, W.; Xu, C.; Shuai, Z.; Gao, M. Polyaniline/Fe3O4 Nanoparticle Composite: Synthesis and Reaction Mechanism. *J. Phys. Chem. B* **2009**, *113* (15), 5052–5058. https://doi.org/10.1021/jp811125k.

(5) Zhang, H.; Zhong, X.; Xu, J.-J.; Chen, H.-Y. Fe3O4/Polypyrrole/Au Nanocomposites with Core/Shell/Shell Structure: Synthesis, Characterization, and Their Electrochemical Properties. *Langmuir* **2008**, *24* (23), 13748–13752. https://doi.org/10.1021/la8028935.

(6) Xuan, S.; Wang, Y.-X. J.; Yu, J. C.; Leung, K. C.-F. Preparation, Characterization, and Catalytic Activity of Core/Shell Fe3O4@polyaniline@Au Nanocomposites. *Langmuir* **2009**, *25* (19), 11835–11843. https://doi.org/10.1021/la901462t.

(7) Guo, J.; Gu, H.; Wei, H.; Zhang, Q.; Haldolaarachchige, N.; Li, Y.; P. Young, D.; Wei, S.; Guo, Z. Magnetite–Polypyrrole Metacomposites: Dielectric Properties and Magnetoresistance Behavior. *J. Phys. Chem. C* **2013**, *117* (19), 10191–10202. https://doi.org/10.1021/jp402236n.

(8) Li, Y.; Chen, G.; Li, Q.; Qiu, G.; Liu, X. Facile Synthesis, Magnetic and Microwave Absorption Properties of Fe3O4/Polypyrrole Core/Shell Nanocomposite. *J. Alloys Compd.* **2011**, *509* (10), 4104–4107. https://doi.org/10.1016/J.JALLCOM.2010.12.100.

(9) Gandhi, N.; Singh, K.; Ohlan, A.; Singh, D. P.; Dhawan, S. K. Thermal, Dielectric and Microwave Absorption Properties of Polyaniline–CoFe2O4 Nanocomposites. *Compos. Sci. Technol.* **2011**, *71* (15), 1754–1760. https://doi.org/10.1016/J.COMPSCITECH.2011.08.010.

(10) Ahmad, H.; Kumar, K.; Rahman, M. A.; Rahman, M. M.; Miah, M. A. J.; Minami, H.; Nuri, M. A. Preparation and Characterization of Conducting Polyaniline Layered Magnetic Nano Composite Polymer Particles. *Polym. Adv. Technol.* **2013**, *24* (8), 740–746. https://doi.org/10.1002/pat.3138.

(11) Radhakrishnan, S.; Rao, C. R. K.; Vijayan, M. Performance of Conducting Polyaniline-DBSA and Polyaniline-DBSA/Fe3O4 Composites as Electrode Materials for Aqueous Redox Supercapacitors. *J. Appl. Polym. Sci.* **2011**, *122* (3), 1510–1518. https://doi.org/10.1002/app.34236.

(12) Chandrasekhar, P. *Conducting Polymers, Fundamentals and Applications*; Springer US: Boston, MA, 1999. https://doi.org/10.1007/978-1-4615-5245-1.

(13) Lizarraga, L.; Andrade, E. M.; Molina, F. V. Swelling and Volume Changes of Polyaniline upon Redox Switching. *J. Electroanal. Chem.* **2004**, *561*, 127–135. https://doi.org/10.1016/J.JELECHEM.2003.07.026.

(14) Antonel, P. S.; Völker, E.; Molina, F. V. Photophysics of Polyaniline: Sequence-Length Distribution Dependence of Photoluminescence Quenching as Studied by Fluorescence Measurements and Monte Carlo Simulations. *Polymer (Guildf).* **2012**, *53* (13), 2619–2627. https://doi.org/10.1016/J.POLYMER.2012.04.041.

(15) De Oliveira, T. V. A. G.; Gobbi, M.; Porro, J. M.; Hueso, L. E.; Bittner, A. M. Charge and Spin Transport in PEDOT:PSS Nanoscale Lateral Devices. *Nanotechnology* **2013**, *24* (47). https://doi.org/10.1088/0957-4484/24/47/475201.

(16) Yamato, H.; Ohwa, M.; Wernet, W. Stability of Polypyrrole and Poly(3,4-Ethylenedioxythiophene) for Biosensor Application. *J. Electroanal. Chem.* **1995**, *397* (1–2), 163–170. https://doi.org/10.1016/0022-0728(95)04156-8.

(17) Aleshin, A. N.; Kiebooms, R.; Heeger, A. J. Metallic Conductivity of Highly Doped Poly(3,4-Ethylenedioxythiophene). *Synth. Met.* **1999**, *101* (1–3), 369–370.

https://doi.org/10.1016/S0379-6779(98)00758-9.

(18) Pei, Q.; Zuccarello, G.; Ahlskog, M.; Inganäs, O. Electrochromic and Highly Stable Poly(3,4-Ethylenedioxythiophene) Switches between Opaque Blue-Black and Transparent Sky Blue. *Polymer (Guildf).* **1994**, *35* (7), 1347–1351. https://doi.org/10.1016/0032-3861(94)90332-8.

(19) Kodama, R. H. Magnetic Nanoparticles. *J. Magn. Magn. Mater.* **1999**, *200* (1–3), 359–372. https://doi.org/10.1016/S0304-8853(99)00347-9.

(20) Beveridge, J. S.; Stephens, J. R.; Williams, M. E. The Use of Magnetic Nanoparticles in Analytical Chemistry. *Annu. Rev. Anal. Chem.* **2011**, *4* (1), 251–273. https://doi.org/10.1146/annurev-anchem-061010-114041.

(21) Mazarío, E.; Herrasti, P.; Morales, M. P.; Menéndez, N. Synthesis and Characterization of CoFe2O4 Ferrite Nanoparticles Obtained by an Electrochemical Method. *Nanotechnology* **2012**, *23* (35), 355708. https://doi.org/10.1088/0957-4484/23/35/355708.

(22) Kim, Y. Il; Kim, D.; Lee, C. S. Synthesis and Characterization of CoFe2O4 Magnetic Nanoparticles Prepared by Temperature-Controlled Coprecipitation Method. *Phys. B Condens. Matter* **2003**, *337* (1–4), 42–51. https://doi.org/10.1016/S0921-4526(03)00322-3.

(23) Singh, K.; Ohlan, A.; Bakhshi, A. K.; Dhawan, S. K. Synthesis of Conducting Ferromagnetic Nanocomposite with Improved Microwave Absorption Properties. *Mater. Chem. Phys.* **2010**, *119* (1–2), 201–207. https://doi.org/10.1016/J.MATCHEMPHYS.2009.08.060.

(24) Bhaumik, M.; Leswifi, T. Y.; Maity, A.; Srinivasu, V. V.; Onyango, M. S. Removal of Fluoride from Aqueous Solution by Polypyrrole/Fe3O4 Magnetic Nanocomposite. *J. Hazard. Mater.* **2011**, *186* (1), 150–159. https://doi.org/10.1016/J.JHAZMAT.2010.10.098.

(25) Shin, S.; Yoon, H.; Jang, J. Polymer-Encapsulated Iron Oxide Nanoparticles as Highly Efficient Fenton Catalysts. *Catal. Commun.* **2008**, *10* (2), 178–182. https://doi.org/10.1016/J.CATCOM.2008.08.027.

(26) Sen, P.; De, A. Electrochemical Performances of Poly(3,4-Ethylenedioxythiophene)-NiFe2O4 Nanocomposite as Electrode for Supercapacitor. *Electrochim. Acta* **2010**, *55* (16), 4677–4684. https://doi.org/10.1016/j.electacta.2010.03.077.

(27) Lu, Z.; Yu, Z.; Dong, J.; Xiong, X.; Gao, L.; Song, M.; Liu, Y.; Fan, D.; Yan, Y.; Huo, P. Enhanced Photocatalytic Activity and Selectivity of a Novel Magnetic PW@PEDOT Imprinted Photocatalyst with Good Reproducibility. *Nano* **2018**, *13* (2), 1–15. https://doi.org/10.1142/S1793292018500200.

(28) Ohlan, A.; Singh, K.; Chandra, A.; Dhawan, S. K. Microwave Absorption Behavior of Core-Shell Structured Poly (3,4-Ethylenedioxy Thiophene)-Barium Ferrite Nanocomposites. *ACS Appl. Mater. Interfaces* **2010**, *2* (3), 927–933. https://doi.org/10.1021/am900893d.

(29) Shin, S.; Jang, J. Thiol Containing Polymer Encapsulated Magnetic Nanoparticles as Reusable and Efficiently Separable Adsorbent for Heavy Metal Ions. *Chem. Commun.* **2007**, No. 41, 4230–4232. https://doi.org/10.1039/b707706h.

(30) Abou-Elazab, T. F.; Migahed, M. D.; Park, H.; Park, Y. W.; MacNeillis, P.; Rabenau, T.; Roth, S. Magnetoresistance of Polypyrrole and Polyacetylene. *Synth. Met.* **1996**, *76* (1–3), 281–284. https://doi.org/10.1016/0379-6779(95)03471-U.

(31) Klemm, P.; Bange, S.; Pöllmann, A.; Boehme, C.; Lupton, J. M. Nanotesla Magnetoresistance in π-Conjugated Polymer Devices. *Phys. Rev. B* **2017**, *95* (24), 241407. https://doi.org/10.1103/PhysRevB.95.241407.

(32) Long, Y.; Chen, Z.; Shen, J.; Zhang, Z.; Zhang, L.; Huang, K.; Wan, M.; Jin, A.; Gu, C.; Duvail, J. L. Magnetoresistance Studies of Polymer Nanotube/Wire Pellets and Single Polymer Nanotubes/Wires. *Nanotechnology* **2006**, *17* (24), 5903–5911. https://doi.org/10.1088/0957-4484/17/24/001.

(33) Chutia, P.; Kumar, A. Temperature- and Magnetic Field-Dependent Electrical Transport Studies of Poly(-3,4 Ethylenedioxythiophene) Nanoparticles. *J. Nanoparticle Res.* **2014**, *16* (9). https://doi.org/10.1007/s11051-014-2617-6.

(34) Gobbi, M.; Orgiu, E. The Rise of Organic Magnetoresistance: Materials and Challenges. *J. Mater. Chem. C* **2017**, *5* (23), 5572–5580. https://doi.org/10.1039/c6tc04403d.

(35) Venkatesan, M.; Nawka, S.; Pillai, S. C.; Coey, J. M. D. Enhanced Magnetoresistance in Nanocrystalline Magnetite. *J. Appl. Phys.* **2003**, *93* (10 3), 8023–8025. https://doi.org/10.1063/1.1555371.

(36) Bhame, S. D.; Joy, P. A. Tuning of the Magnetostrictive Properties of CoFe2O4 by Mn Substitution for Co. *J. Appl. Phys.* **2006**, *100* (11), 1–5. https://doi.org/10.1063/1.2401648.

(37) Msomi, J. Z.; Moyo, T.; Abdallah, H. M. I.; Dolo, J. J. Electrical and Magnetoresistance

Properties of MgxMn1-XFe2O4 Compounds. *J. Supercond. Nov. Magn.* **2013**, *26* (4), 1021–1025. https://doi.org/10.1007/s10948-012-1988-0.

(38) Majumdar, S.; Grochowska, K.; Sawczak, M.; Ƚliwiński, G.; Huhtinen, H.; Dahl, J.; Tuominen, M.; Laukkanen, P.; Majumdar, H. S. Interfacial Properties of Organic Semiconductor-Inorganic Magnetic Oxide Hybrid Spintronic Systems Fabricated Using Pulsed Laser Deposition. *ACS Appl. Mater. Interfaces* **2015**, *7* (40), 22228–22237. https://doi.org/10.1021/acsami.5b04840.

(39) Gu, H.; Zhang, X.; Wei, H.; Huang, Y.; Wei, S.; Guo, Z. An Overview of the Magnetoresistance Phenomenon in Molecular Systems. *Chem. Soc. Rev.* **2013**, *42* (13), 5907–5943. https://doi.org/10.1039/c3cs60074b.

(40) Guo, L.; Gu, X.; Zhu, X.; Sun, X. Recent Advances in Molecular Spintronics: Multifunctional Spintronic Devices. *Adv. Mater.* **2019**, *1805355*, 1–8. https://doi.org/10.1002/adma.201805355.

(41) Romero, M.; Faccio, R.; Pardo, H.; Tumelero, M. A.; Montenegro, B.; Campos Plá Cid, C.; Pasa, A. A.; Mombrú, Á. W. The Effect of Manganite Nanoparticle Addition on the Low Field Magnetoresistance of Polyaniline. *J. Mater. Chem. C* **2015**, *3* (46), 12040–12047. https://doi.org/10.1039/c5tc03083h.

(42) Gu, H.; Huang, Y.; Zhang, X.; Wang, Q.; Zhu, J.; Shao, L.; Haldolaarachchige, N.; Young, D. P.; Wei, S.; Guo, Z. Magnetoresistive Polyaniline-Magnetite Nanocomposites with Negative Dielectrical Properties. *Polymer (Guildf).* **2012**, *53* (3), 801–809. https://doi.org/10.1016/J.POLYMER.2011.12.033.

(43) Paterno, L. G.; Soler, M. A. G.; Fonseca, F. J.; Sinnecker, J. P.; Sinnecker, E. H. C. P.; Lima, E. C. D.; Novak, M. A.; Morais, P. C. Layer-by-Layer Assembly of Bifunctional Nanofilms: Surface-Functionalized Maghemite Hosted in Polyaniline. *J. Phys. Chem. C* **2009**, *113* (13), 5087–5095. https://doi.org/10.1021/jp8092463.

(44) Soler, M. A. G.; Paterno, L. G.; Sinnecker, J. P.; Wen, J. G.; Sinnecker, E. H. C. P.; Neumann, R. F.; Bahiana, M.; Novak, M. A.; Morais, P. C. Assembly of γ-Fe2O3/Polyaniline Nanofilms with Tuned Dipolar Interaction. *J. Nanoparticle Res.* **2012**, *14* (2). https://doi.org/10.1007/s11051-011-0653-z.

(45) Muñoz Resta, I.; Sellés, J. M.; Lanús Méndez Elizalde, M.; Antonel, P. S.; Molina, F. V. Polypyrrole-CoFe2O4 Nanocomposites: Polymer Influence on Magnetic Behavior and Particle Effects on Polymer Conduction. *Polym. Compos.* **2018**, *39* (12), 4617–4627. https://doi.org/10.1002/pc.24575.

(46) Zhou, W.; Hu, X.; Bai, X.; Zhou, S.; Sun, C.; Yan, J.; Chen, P. Synthesis and Electromagnetic, Microwave Absorbing Properties of Core-Shell Fe3O4-Poly(3,4-Ethylenedioxythiophene) Microspheres. *ACS Appl. Mater. Interfaces* **2011**, *3* (10), 3839–3845. https://doi.org/10.1021/am2004812.

(47) Antonel, P. S.; Jorge, G.; Perez, O. E.; Butera, A.; Leyva, A. G.; Negri, R. M. Magnetic and Elastic Properties of CoFe2O4 - Polydimethylsiloxane Magnetically Oriented Elastomer Nanocomposites. *J. Appl. Phys.* **2011**, *110* (4), 043920. https://doi.org/10.1063/1.3624602.

(48) Ohlan, A.; Singh, K.; Chandra, A.; Dhawan, S. K. Microwave Absorption Behavior of Core - Shell Structured Poly (3,4 - Ethylenedioxy Thiophene) - Barium Ferrite

Nanocomposites. *ACS Appl. Mater. Interfaces* **2010**, *2* (3), 927–933. https://doi.org/10.1021/am900893d.

(49) Schulman, A.; Lanosa, L. F.; Acha, C. Poole-Frenkel Effect and Variable-Range Hopping Conduction in Metal/YBCO Resistive Switching Devices. *J. Appl. Phys.* **2015**, *118* (4), 2–8. https://doi.org/10.1063/1.4927522.

(50) Klemm, P.; Bange, S.; Pöllmann, A.; Boehme, C.; Lupton, J. M. Nanotesla Magnetoresistance in π-Conjugated Polymer Devices. *Phys. Rev. B* **2017**, *95* (24), 1–6. https://doi.org/10.1103/PhysRevB.95.241407.

(51) Qu, Y.; Yang, H.; Yang, N.; Fan, Y.; Zhu, H.; Zou, G. The Effect of Reaction Temperature on the Particle Size, Structure and Magnetic Properties of Coprecipitated CoFe2O4 Nanoparticles. *Mater. Lett.* **2006**, *60* (29–30), 3548–3552. https://doi.org/10.1016/J.MATLET.2006.03.055.

(52) Hu, J.-M.; Sheng, G.; Zhang, J. X.; Nan, C. W.; Chen, L. Q. Phase-Field Simulation of Strain-Induced Domain Switching in Magnetic Thin Films. *Appl. Phys. Lett.* **2011**, *98* (11), 112505. https://doi.org/10.1063/1.3567542.

(53) Gajbhiye, N. S.; Prasad, S.; Balaji, G. Experimental Study of Hopkinson Effect in Single Domain CoFe2O4 Particles. *IEEE Trans. Magn.* **1999**, *35* (4), 2155–2161. https://doi.org/10.1109/20.774187.

(54) Sun, S.; Zeng, H.; Robinson, D. B.; Raoux, S.; Rice, P. M.; Wang, S. X.; Li, G. Monodisperse MFe_2O_4 (M = Fe, Co, Mn) Nanoparticles. *J. Am. Chem. Soc.* **2004**, *126* (1), 273–279. https://doi.org/10.1021/ja0380852.

(55) Kambale, R. C.; Shaikh, P. A.; Harale, N. S.; Bilur, V. A.; Kolekar, Y. D.; Bhosale, C. H.; Rajpure, K. Y. Structural and Magnetic Properties of Co1-XMnxFe2O4 ($0 \leq x \leq 0.4$) Spinel Ferrites Synthesized by Combustion Route. *J. Alloys Compd.* **2010**, *490* (1–2), 568–571. https://doi.org/10.1016/j.jallcom.2009.10.082.

(56) Awad, K. R.; Wahsh, M. M. S.; Othman, A. G. M.; Girgis, E.; Mabrouk, M. R.; Morsy, F. A. Effect of Mn2+ Doping and SiO2 Coating on Magneto-Optical Properties of CoFe2O4 Nano-Particles. *Smart Mater. Struct.* **2015**, *24* (11), 115002. https://doi.org/10.1088/0964-1726/24/11/115002.

(57) Kurian, M.; Thankachan, S.; Nair, D. S.; E. K, A.; Babu, A.; Thomas, A.; Krishna K. T, B. Structural, Magnetic, and Acidic Properties of Cobalt Ferrite Nanoparticles Synthesised by Wet Chemical Methods. *J. Adv. Ceram.* **2015**, *4* (3), 199–205. https://doi.org/10.1007/s40145-015-0149-x.

(58) Choi, J. W.; Han, M. G.; Kim, S. Y.; Oh, S. G.; Im, S. S. Poly(3,4-Ethylenedioxythiophene) Nanoparticles Prepared in Aqueous DBSA Solutions. *Synth. Met.* **2004**, *141* (3), 293–299. https://doi.org/10.1016/S0379-6779(03)00419-3.

(59) Morvant, M. C.; Reynolds, J. R. In Situ Conductivity Studies of Poly(3,4-Ethylenedioxythiophene). *Synth. Met.* **1998**, *92* (1), 57–61. https://doi.org/10.1016/S0379-6779(98)80023-4.

(60) Corradi, R.; Armes, S. P. Chemical Synthesis of Poly(3,4-Ethylenedioxythiophene). *Synth. Met.* **1997**, *84* (1–3), 453–454.

(61) McLachlan, D. S. An Equation for the Conductivity of Binary Mixtures with Anisotropic

Grain Structures. *J. Phys. C Solid State Phys.* **1987**, *20* (7), 865–877. https://doi.org/10.1088/0022-3719/20/7/004.

(62) McLachlan, D. S.; Blaszkiewicz, M.; Newnham, R. E. Electrical Resistivity of Composites. *J. Am. Ceram. Soc.* **1990**, *73* (8), 2187–2203. https://doi.org/10.1111/j.1151-2916.1990.tb07576.x.

(63) Kumar, S. S.; Kumar, C. S.; Mathiyarasu, J.; Phani, K. L. Stabilized Gold Nanoparticles by Reduction Using 3,4- Ethylenedioxythiophene-Polystyrenesulfonate in Aqueous Solutions: Nanocomposite Formation, Stability, and Application in Catalysis. *Langmuir* **2007**, *23* (6), 3401–3408. https://doi.org/10.1021/la063150h.

(64) Selvaganesh, S. V.; Mathiyarasu, J.; Phani, K. L. N.; Yegnaraman, V. Chemical Synthesis of PEDOT-Au Nanocomposite. *Nanoscale Res. Lett.* **2007**, *2* (11), 546–549. https://doi.org/10.1007/s11671-007-9100-6.

(65) Chinnasamy, C. N.; Jeyadevan, B.; Shinoda, K.; Tohji, K.; Kasuya, A. Growth Dominant Co-Precipitation Process to Achieve High Coercivity at Room Temperature in CoFe 2 O 4 Nanoparticles. *IEEE Trans. Magn.* **2002**, *38* (1), 2640–2642. https://doi.org/10.1109/TMAG.2002.801972.

(66) Leslie-Pelecky, D. L.; Rieke, R. D. Magnetic Properties of Nanostructured Materials. *Chem. Mater.* **1996**, *8* (8), 1770–1783. https://doi.org/10.1021/cm960077f.

(67) Safi, R.; Ghasemi, A.; Shoja-Razavi, R.; Tavousi, M. The Role of PH on the Particle Size and Magnetic Consequence of Cobalt Ferrite. *J. Magn. Magn. Mater.* **2015**, *396*, 288–294. https://doi.org/10.1016/j.jmmm.2015.08.022.

(68) Zhang, H.; Zeng, D.; Liu, Z. The Law of Approach to Saturation in Ferromagnets Originating from the Magnetocrystalline Anisotropy. *J. Magn. Magn. Mater.* **2010**, *322* (16), 2375–2380. https://doi.org/10.1016/J.JMMM.2010.02.040.

(69) Muñoz Resta, I.; Horwitz, G.; Lanus Mendez Elizalde, M.; Jorge, G. A.; Molina, F. V.; Antonel, P. S. Magnetic and Conducting Properties of Composites of Conducting Polymers and Ferrite Nanoparticles. *IEEE Trans. Magn.* **2013**, *49* (8), 4598–4601. https://doi.org/10.1109/TMAG.2013.2259582.

(70) Kittel, C. Quantum Theory of Solids, 2nd Revised Edition; John Wiley & Sons, Ltd: Hoboken, 1987; Chapt. 18.

(71) Shi, W.; Zhao, T.; Xi, J.; Wang, D.; Shuai, Z. Unravelling Doping Effects on PEDOT at the Molecular Level: From Geometry to Thermoelectric Transport Properties. *J. Am. Chem. Soc.* **2015**, *137* (40), 12929–12938. https://doi.org/10.1021/jacs.5b06584.

(72) Wei, Q.; Mukaida, M.; Ishida, T. Extracting Carrier Mobility in Conducting Polymers Using a Photoinduced Charge Transfer Reaction. *J. Phys. Chem. C* **2018**, *122* (28), 15922–15928. https://doi.org/10.1021/acs.jpcc.8b04885.

(73) Gueye, M. N.; Carella, A.; Faure-Vincent, J.; Demadrille, R.; Simonato, J. P. Progress in Understanding Structure and Transport Properties of PEDOT-Based Materials: A Critical Review. *Prog. Mater. Sci.* **2020**, *108* (November 2019), 100616. https://doi.org/10.1016/j.pmatsci.2019.100616.

(74) El-Sayed, H. M. Evidence on the Presence of Ruderman–Kittel–Kasuya–Yosida (RKKY) Interaction in CoFe2O4@Au Nano Structure. *Superlattices Microstruct.* **2016**, *91*, 98–

104. https://doi.org/10.1016/J.SPMI.2016.01.009.

(75) García-Otero, J.; Porto, M.; Rivas, J. Henkel Plots of Single-Domain Ferromagnetic Particles. *J. Appl. Phys.* **2000**, *87* (10), 7376–7381. https://doi.org/10.1063/1.372996.

(76) Wohlfarth, E. P. Relations between Different Modes of Acquisition of the Remanent Magnetization of Ferromagnetic Particles. *J. Appl. Phys.* **1958**, *29* (3), 595–596. https://doi.org/10.1063/1.1723232.

(77) Che, X.; Neal Bertram, H. Phenomenology of ΔM Curves and Magnetic Interactions. *J. Magn. Magn. Mater.* **1992**, *116* (1–2), 121–127. https://doi.org/10.1016/0304-8853(92)90155-H.

TOC Graphic

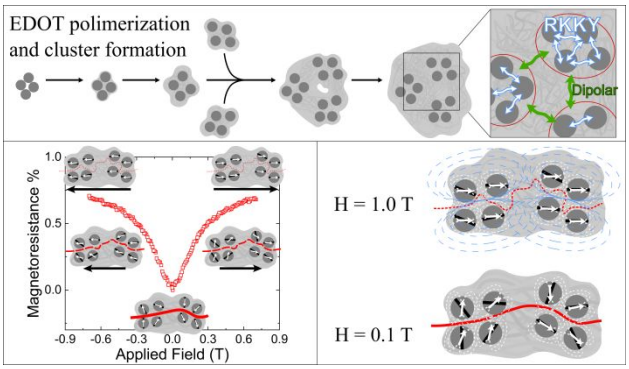

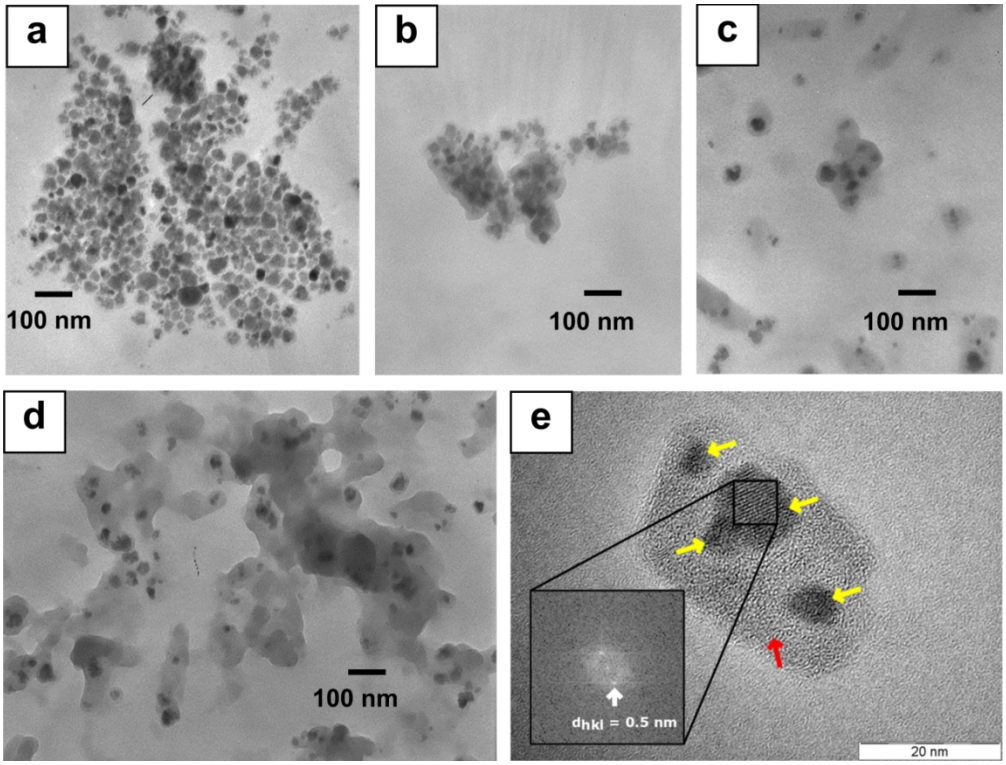

TEM and HR-TEM images of CoFe2O4 nanoparticles and CoFe2O4-PEDOT composites

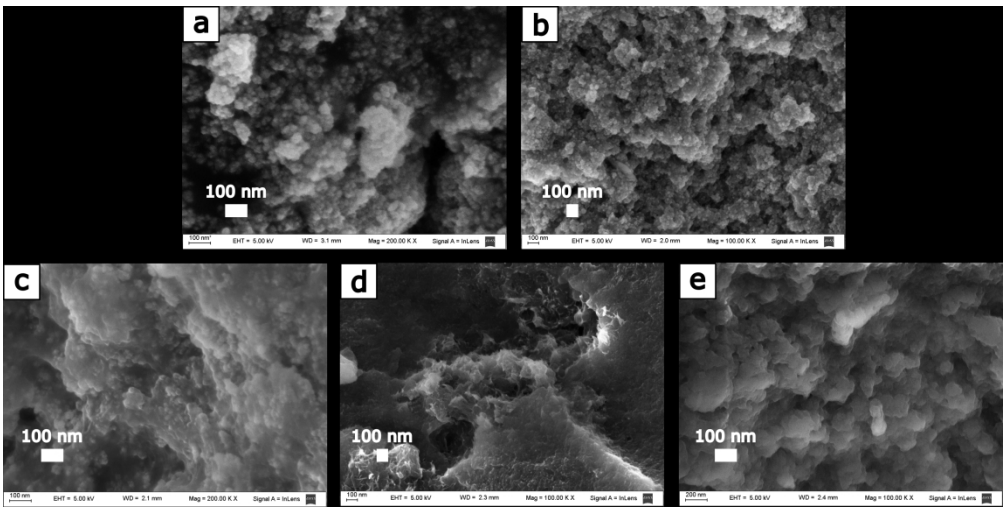

SEM images of CoFe2O4-PEDOT composites

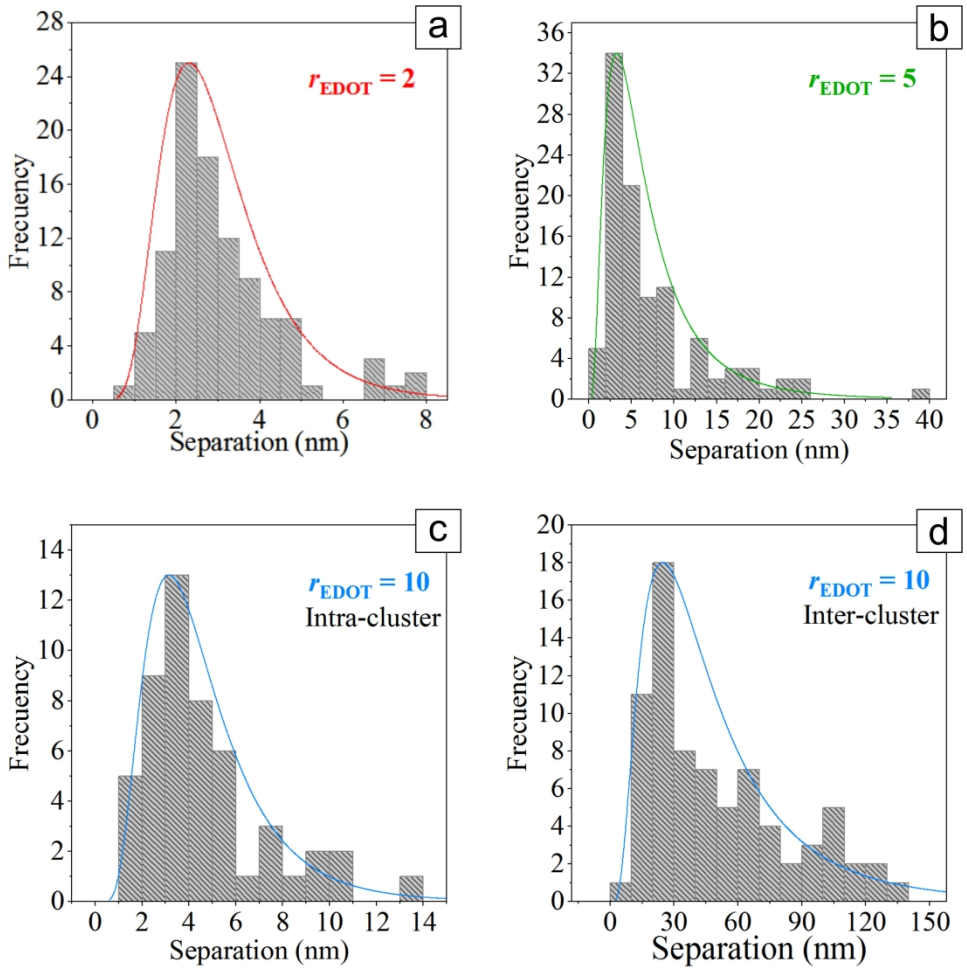

Particle-particle separation for CoFe2O4-PEDOT composites

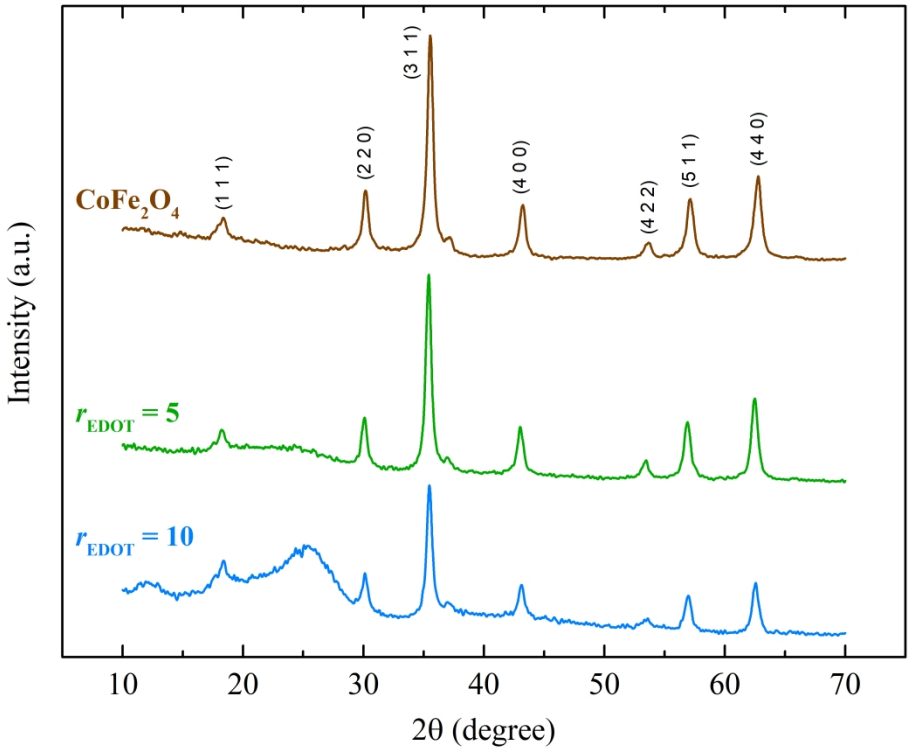

XRD diagram/patterns of CoFe2O4 nanoparticles and composites for different rEDOT ratios. Nanoparticles synthesized at 80 ºC reveals an inverse spinel structure

89x68mm (1200 x 1200 DPI)

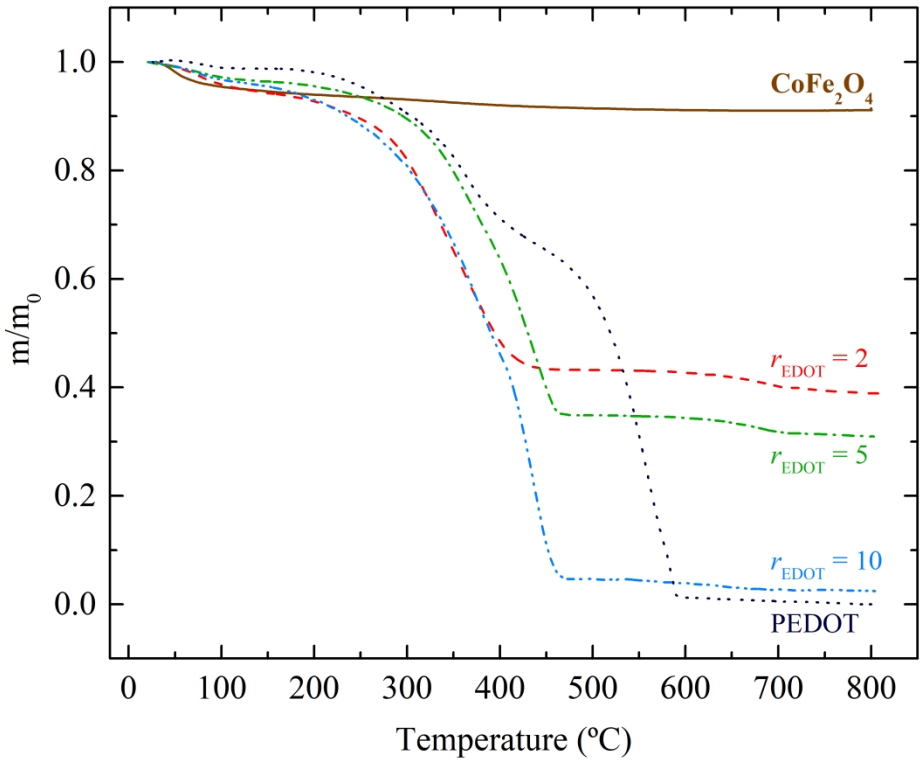

TGA measurements of cobalt ferrite, PEDOT and composites, plotted as relative mass (m/m0) as a function of temperature

89x72mm (1200 x 1200 DPI)

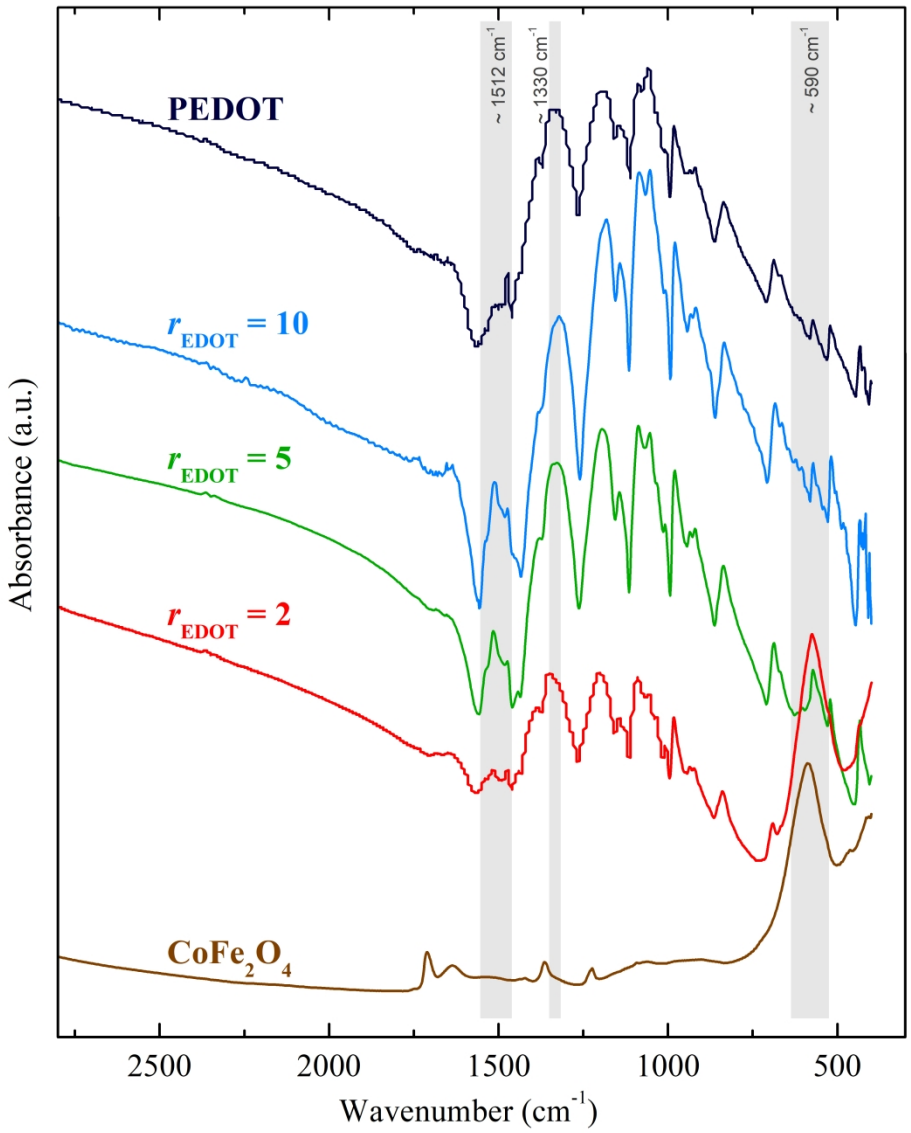

IR spectra of PEDOT, CoFe2O4 nanoparticles and composites PEDOT-CoFe2O4 with different rEDOT ratio

89x106mm (1200 x 1200 DPI)

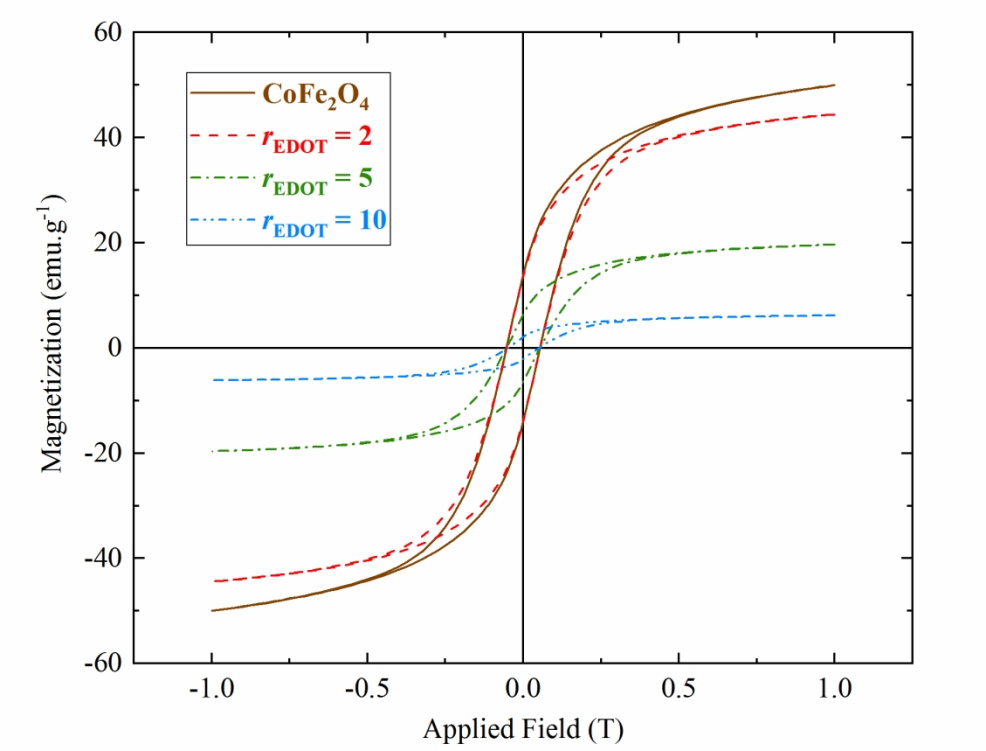

Magnetization curves of CoFe2O4 particles and composites with different rEDOT

84x64mm (600 x 600 DPI)

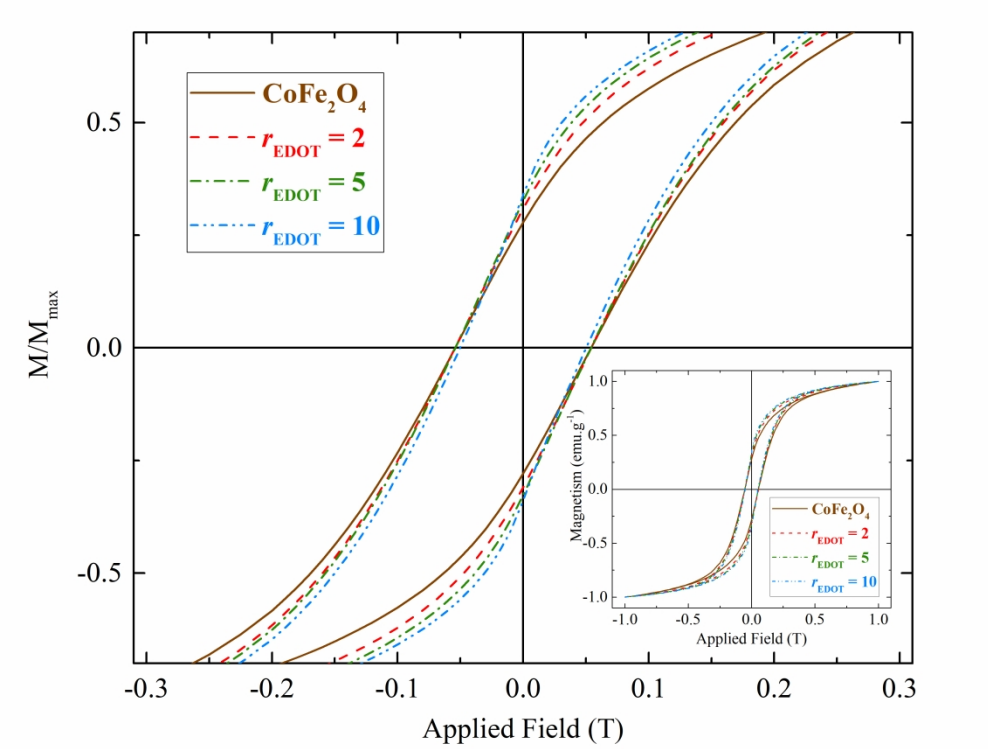

Normalized magnetization curves for CoFe2O4-PEDOT composites, for different rEDOT. The insets show the full curves, and the main graphs present an enlargement about H = 0

84x64mm (1200 x 1200 DPI)

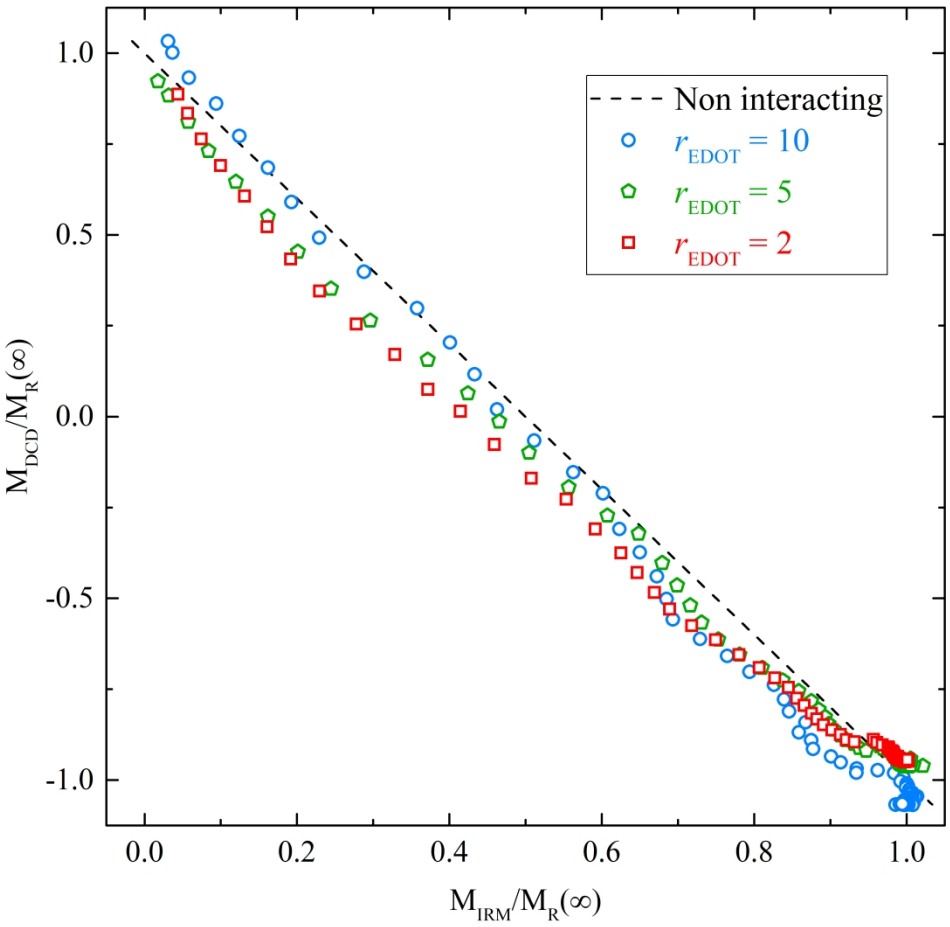

Henkel Plot for CoFe2O4-PEDOT composites with different rEDOT ratios

89x89mm (1200 x 1200 DPI)

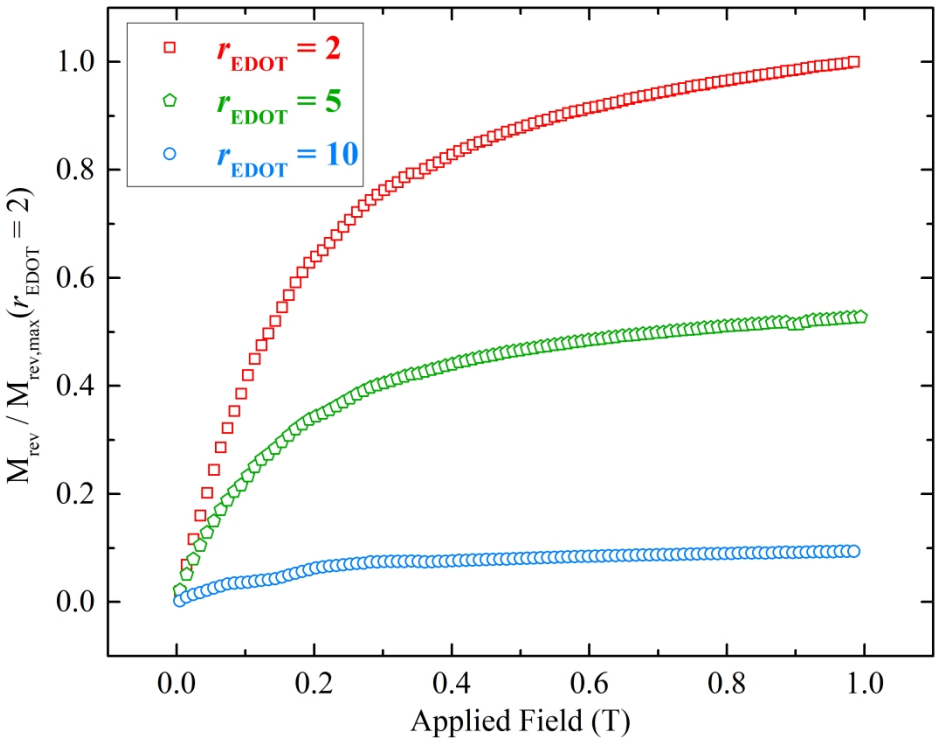

Normalized reversible magnetization for CoFe2O4-PEDOT composites with different rEDOT ratios

89x68mm (1200 x 1200 DPI)

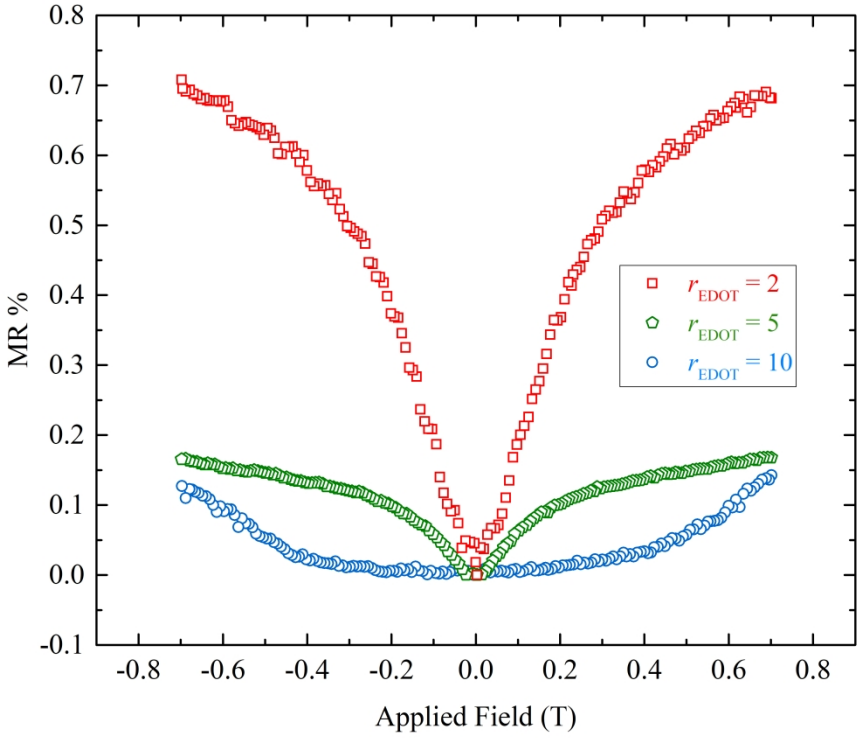

Magnetoresistance for CoFe2O4-PEDOT composites with different rEDOT ratios

89x68mm (1200 x 1200 DPI)

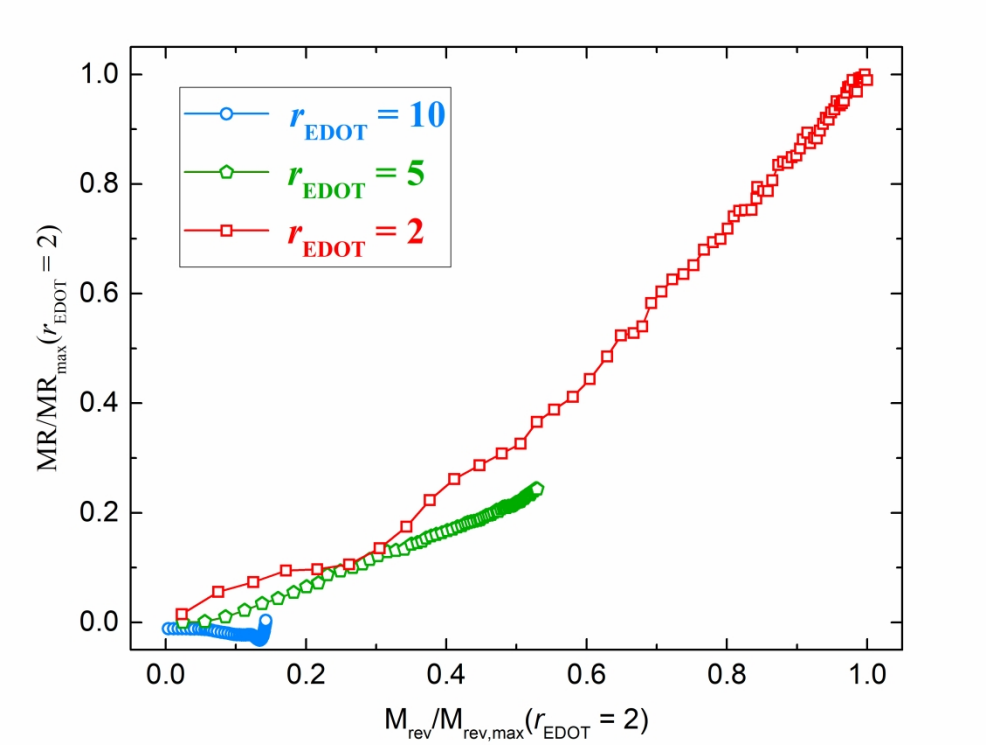

Normalized Relative Magnetoresistance vs. Relative Reversible magnetization for CoFe2O4-PEDOT composites with different rEDOT molar ratios

84x64mm (1200 x 1200 DPI)